CHEMICAL REVIEWS

pubs.acs.org/CR

Review

Electrochemical Carbon Dioxide Capture and Concentration

Alessandra M. Zito,[‖] Lauren E. Clarke,[‖] Jeffrey M. Barlow,[‖] Daniel Bím,[‖] Zisheng Zhang, Katelyn M. Ripley, Clarabella J. Li, Amanda Kummeth, McLain E. Leonard, Anastassia N. Alexandrova,* Fikile R. Brushett,* and Jenny Y. Yang*

Cite This: *Chem. Rev.* 2023, 123, 8069–8098

Read Online

ACCESS | Metrics & More | Article Recommendations

ABSTRACT: Electrochemical carbon capture and concentration (eCCC) offers a promising alternative to thermochemical processes as it circumvents the limitations of temperature-driven capture and release. This review will discuss a wide range of eCCC approaches, starting with the first examples reported in the 1960s and 1970s, then transitioning into more recent approaches and future outlooks. For each approach, the achievements in the field, current challenges, and opportunities for improvement will be described. This review is a comprehensive survey of the eCCC field and evaluates the chemical, theoretical, and electrochemical engineering aspects of different methods to aid in the development of modern economical eCCC technologies that can be utilized in large-scale carbon capture and sequestration (CCS) processes.

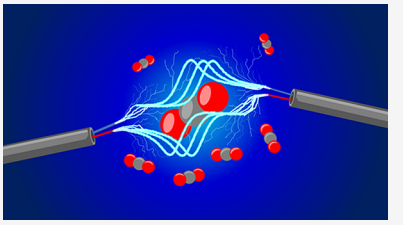

CONTENTS

1. INTRODUCTION

Burgeoning population and industrialization have resulted in significantly increased global energy demand and fossil fuel consumption. As a result, anthropogenic carbon dioxide (CO_2) emissions have quickly grown to unsustainable levels. Despite aggressive targets and policies implemented globally to reduce emissions over the last several years, our annual rate of net CO_2 released has reached record levels, exceeding 36 Gt CO_2/year from fossil fuels and industry in both 2019 and 2021.[1−3] To limit global temperature rise to well below 2 °C, as called

Received: October 20, 2022
Published: June 21, 2023

for by the 2015 Paris agreement,[4] rapid and widespread decarbonization efforts are needed across all sectors of our economy.

Transitioning toward a decarbonized society will need to be driven by a significant expansion of renewables and electrification, coupled with energy efficiency improvements. However, pathways for reducing emissions to achieve our global climate goals also call for large scale carbon capture and storage (CCS) or utilization/conversion (CCU).[1,4,5] Different approaches for carbon capture allow for mitigating CO_2 emissions across a variety of sectors. In 2019, the power (i.e., electricity, heat) and industrial/manufacturing sectors accounted for over 60% of the CO_2 emitted worldwide.[6] Within these sectors, large scale stationary "point-sources" make up the majority of these emissions, which are generated from burning fossil fuels in power plants/large industrial plants or as chemical process byproducts. Postcombustion capture is a common approach to address large point-sources from fossil fuel-based infrastructure, where CO_2 is removed from the generated flue gas. Similar technologies can also be employed for hard-to-decarbonize industrial processes with CO_2-generating reactions (e.g., cement production).[7] The other ca. 40% of global CO_2 emissions are mainly generated by the transportation, buildings, and land-use/forestry sectors. These are often referred to as "nonpoint sources" as they primarily consist of small, disperse, and often mobile emissions.[2,6] While existing technologies are generally not equipped to effectively capture CO_2 from nonpoint-source emitters, direct air capture (DAC) has been proposed as one viable approach, where CO_2 is extracted from the atmosphere. Long-term operation of DAC can even lead to a net-negative future, where more CO_2 is removed from the air as compared to what is released.[8,9]

Considerable progress has been made in the development and optimization of carbon capture systems, particularly for coal and natural gas power plant applications.[1] According to the Global CCS institute, more than 100 commercial scale CCS facilities are operational, in construction, or in development stages as of 2021, most of which capture CO_2 from the power and industrial sectors with postcombustion capture technologies.[10] However, in order to meet the Paris agreement, not only would all "point-source" processes need to approach net-zero carbon emissions, but emissions from other distributed sources also need to be significantly reduced or eliminated.[11] As described above, DAC systems can account for "nonpoint sources". While there are currently fewer commercialized DAC processes (18 plants operating worldwide in 2023), and those that do exist are relatively small-scale, DAC is currently receiving increased levels of attention and monetary support from both public- and private-sector organizations.[12]

Despite the role CCS is projected to play in emissions reduction, a major drawback to current technologies is that carbon capture and concentration (CCC) methods remain energy-intensive and costly, preventing widespread implementation.[13−17] One of the most mature CCC technologies is the utilization of amine-based absorbent solutions for capture from power plant flue gas. Such a process exploits the natural affinity of amines for absorbing CO_2 at room temperature, followed by the thermal regeneration of the absorber to enable cyclic use.[18] A weakness of this approach, and thermally driven separation in general, is the Carnot limitation incurred by the temperature swings necessary for absorption and desorption. As a result, a typical alkanolamine capture process operating between ∼37−117 °C can only approach a maximum of ∼21% energetic efficiency.[19] After decades of research, most state-of-the-art amine capture systems still have high heating demands of ≥2.3 GJ/metric ton CO_2 (≥100 kJ/mol CO_2). Therefore, current systems are limited to ≤22% of the Carnot efficiency, or <5% overall energetic efficiency, upon optimization at scale.[20−23] To put this efficiency into context, 20−30% of the entire power output of a typical coal-fired power plant is required to power a retrofitted CCC process alone.[24,25] Using these systems, every ton of captured CO_2 would cost an estimated $50−100 for power generation plants and $40−120 for industrial sources (i.e., cement, iron, or steel).[26−29] CCC systems for DAC are further underdeveloped, and the energy requirements are much higher due to the significantly lower CO_2 concentrations. It is estimated that existing thermochemical DAC systems require ≥4.3 GJ/ton CO_2 (or ≥190 kJ/mol CO_2), operating at ≤10% of the energetic efficiency, resulting in higher system costs; however, it is important to note that due to the early development stage of DAC technologies, these energy estimates are generated with less certainty than point-source capture facilities.[14,30] Reported DAC cost estimates are in the range of $130−1000/ton CO_2, dependent upon the source of heat to drive regeneration (i.e., waste heat or generated heat) and the carbon footprint associated with this heat.[14,29−32] Specifically, methods which fall on the lower end of this cost range typically assume access to a source of waste heat to carry out process heating needs. Reaching net-zero emissions by 2040 is estimated to require about 2000 large-scale CCS facilities worldwide.[33] While most current commercial demonstrations primarily use thermochemical approaches, achievement of large-scale carbon capture will likely require a diverse portfolio of options. Development of methods which offer higher energetic efficiencies than thermally driven processes and are operated with low-carbon energy sources could enable more widespread deployment of CCC.

More efficient CO_2 separation strategies would specifically enable operation closer to the thermodynamic minimum for system energy requirements. To separate a species from a gaseous mixture, the minimum energy is equal to the difference in Gibbs free energy before and after separation. In the limit of "skimming", where an infinitesimal quantity of CO_2 is removed from a feed gas mixture at ambient pressures, the Gibbs free energy of separation (ΔG) is given by eq 1.[34]

$$\Delta G = -RT \ln\left(\frac{P_{CO_2}}{P_0}\right) \tag{1}$$

where R is the ideal gas constant (8.314 J mol^{-1} K^{-1}), T is the absolute temperature (K), P_{CO_2} is the partial pressure of CO_2 in the feed gas mixture, and P_0 is the ambient pressure. The relationship between the change in free energy and partial pressure demonstrates that CO_2 separation is an endergonic process whose energetics depend on the reaction conditions as well as the required changes in concentration. For example, for DAC, separating 400 ppm of CO_2 from air at standard temperature (T = 298.15 K) and pressure (1 bar) to generate a pure CO_2 stream at 1 bar will require at least 19.4 kJ/mol CO_2. Additionally, concentration from a flue gas stream containing 15 mol % CO_2 at ambient conditions requires a minimum work of separation of 4.7 kJ/mol CO_2. Note that "skimming" considered in eq 1 represents a lower bound of energy requirements, which will increase with the fraction of CO_2 removed from the feed gas. Considering 90% removal of CO_2

https://doi.org/10.1021/acs.chemrev.2c00681
Chem. Rev. 2023, 123, 8069−8098

from a flue gas mixture (15 mol % CO_2), and using expressions demonstrated in previous work,[14,34] at least 6.4 kJ/mol CO_2 is required. The minimum thermodynamic work constitutes a limit which is unachievable under practical conditions due to irreversible losses (e.g., entropic losses); however, all processes, whether they are thermochemical, electrochemical, or otherwise, aim to balance these losses with process efficiency, selectivity, and yield, with a goal of minimizing cost.

Electrochemical carbon capture and concentration (eCCC) offers a promising alternative to thermochemical processes as it circumvents the limitations of temperature-driven capture and release.[35−39] More specifically, electrochemical carbon capture systems are not bounded by Carnot efficiencies and can theoretically approach operation at the thermodynamic minimum energy requirement (i.e., 100% energetic efficiencies).[37] As such, in electrochemical systems, the minimum cell potential (E_{cell}, eq 2) is related to the minimum separation work (represented by the change in Gibbs free energy).

$$E_{cell} = -\frac{\Delta G}{nF} \tag{2}$$

where n is the moles of electrons transferred per mole of CO_2 captured, F is the Faraday constant (96485 C mol^{-1}), and together, they describe the charge transferred during the reaction. As CO_2 separation is a nonspontaneous process ($\Delta G > 0$), the cell potential, or difference between the potential of the cathode and anode, is negative ($E_{cell} < 0$). This minimum cell potential is directly related to the relative CO_2 concentrations at the two electrodes *via* the Nernst equation. To perturb the reaction equilibrium and drive the process toward favorable CO_2 separation, the actual cell voltage magnitude ($|V_{cell}|$) must be greater than $|E_{cell}|$, resulting in energetic losses. This deviation from E_{cell} is dependent on the thermodynamic cycle of the separation system and overpotentials that result from resistive losses in the electrochemical cell(s). These cell resistances arise from a summation of inefficiencies associated with kinetic, ohmic, and transport phenomena that underlie system operation and their magnitudes are influenced by the chosen cell materials and reactor operating conditions (i.e., current density). Thus, cell potential and associated energy requirements are influenced by several design and operational factors. Despite these potential energetic penalties, an advantage of electrochemical systems is their ability to apply electric currents (*via* polarized electrode surfaces) that directly act on target redox-active molecules rather than on the entire capture medium via heating and cooling, thus reducing or eliminating sensible heat losses. Due to these differences in process energetics, electrochemical systems can potentially operate with reduced energy requirements over thermochemical systems and are therefore particularly attractive. Additionally, eCCC systems present an opportunity to operate at milder conditions (i.e., at or near room temperature), allow for modular designs that can more readily be scaled up or down, and can run on electricity from renewable sources.

This review will begin by providing a timeline and overview of eCCC (section 2), describing early work in the field and the motivation for pursuing such a process, outlining current eCCC approaches, and highlighting important metrics for assessing these systems. We will then transition toward discussing each of the current approaches more in depth, with a heavier emphasis on methods that employ redox mediators to facilitate CO_2 capture and release. These methods rely more on optimization through chemical design and include pH-mediated systems (section 3), electrochemically mediated amine regeneration (section 4), and direct capture with redox-active molecules (section 5). For each approach, we provide a general overview of the system, discuss redox mediator chemistries that have been studied in literature, and highlight requirements for future generations of redox mediators. We then discuss previous demonstrations of each method, briefly highlight important considerations for cell/system design, and describe current cell/system platforms that have been used at the lab-scale. To conclude (section 6), we summarize achievements in the field, current challenges, and opportunities for improving these technologies. Overall, this review is a comprehensive survey of the eCCC field and evaluates the chemical, theoretical, and electrochemical engineering aspects of this approach. We hope this work can be used to assist the community in the development of modern economical eCCC technologies that can be utilized in large-scale CCS/CCU processes.

2. TIMELINE AND OVERVIEW OF ECCC

2.1. Early Work and Motivation

eCCC uses electron transfer reactions to drive CO_2 separation. The original motivation for using an electrochemical approach to CCC can be traced back to 1969, when Huebscher and Babinsky were interested in developing an efficient way to separate carbon dioxide from the atmosphere to be used for life support systems, specifically for use in submarines as well as air and space travel.[40] Their system can operate continuously and includes two electrochemical concentration cell stacks, a process air blower, and a dehumidifying−humidifying unit (Figure 1). The process of CO_2 separation can be broken

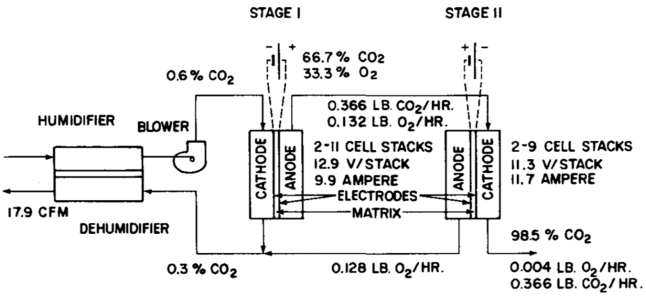

Figure 1. Huebscher and Babinsky model for the first known eCCC system. Reproduced with permission from ref 40. Copyright 1969 SAE International.

down into two stages, which are both typically operated at temperatures of 65 °C or lower. The first stage (stage I, Figure 1) features the carbonation cell, in which a CO_2-rich air stream (0.6%) is supplied to the cathode, where both CO_2 and oxygen (O_2) are removed (Scheme 1, cathodic reactions). Then, a concentrated mixture of CO_2 (66.7%) and O_2 (33.3%) is generated at the anode (Scheme 1, anodic reactions).

Because the first stage captures both oxygen and carbon dioxide, the second stage (stage II, Figure 1) is used for their separation. The cell is similar to the carbonation cell in stage I, but it uses an acidic electrolyte, such that oxygen is reduced at the cathode and reacts with protons to form water (i.e., $O_2 + 4H^+ + 4e^- \rightarrow 2H_2O$). The reduction step removes oxygen so that CO_2 can be recovered at high purities. At the anode of the stage II cell, water decomposes *via* oxidation to reform oxygen

https://doi.org/10.1021/acs.chemrev.2c00681
Chem. Rev. 2023, 123, 8069−8098

Scheme 1. Reactions Governing Huebscher and Babinsky's Low-Temperature Carbonation Cell[4]

Cathodic Reactions	Anodic Reactions
$O_2 + 2H_2O + 4e^- \rightarrow 4OH^-$	$4OH^- \rightarrow O_2 + 2H_2O + 4e^-$
$CO_2 + OH^- \rightarrow HCO_3^-$	$CO_3^{2-} + H_2O \rightarrow HCO_3^- + OH^-$
$HCO_3^- + OH^- \rightarrow CO_3^{2-} + H_2O$	$HCO_3^- \rightarrow CO_2 + OH^-$

and protons (H^+); the O_2 is transferred out of the cell, and the protons are reconsumed at the cathode.

This system captured CO_2 from low levels with concentration at high purities (97−98%) and was stable for over 1000 h of operation. Additionally, this system was similar or lighter in weight than other systems at the time,[41,42] making it an effective option for mobile applications. However, the process is energy intensive, requiring cell voltages ca. ≥1 V for both stage I and stage II. This voltage is quite high, considering that the minimum cell voltage for separating 0.6% CO_2 is ca. 0.1 V (from eq 1 and 2). Despite these limitations associated with Huebscher and Babinsky's system, it was the first demonstration of electrochemical CO_2 capture and concentration.

Later, in 1971, Wynveen and Quattrone used an ambient-temperature eCCC system for aircrafts,[43] which was also demonstrated by Wynveen *et al.* for spacecrafts.[44] Winnick *et al.* also explored the use of this system for O_2 regeneration during manned space missions using carbon capture, concentration, and conversion.[45] Wynveen and Quattrone's technology contained electrochemical cells operating continuously in series, where each used an aqueous cesium carbonate (Cs_2CO_3) electrolyte. The electrodes were made of a fine mesh onto which Teflon and platinum were cast, forming a porous platinum electrode. The setup was similar to that of a fuel cell, where the cathode and anode were separated by the electrolyte (supported by a porous matrix), and gas-phase reactants were fed directly to the electrodes. The feed gas on the cathode side was humid, CO_2-containing cabin air. The cathode had a similar function to the stage I cathode of the Huebscher and Babinsky method described above (Scheme 1), where both CO_2 and O_2 are reduced and thus captured. On the anode side, hydrogen is fed to the cell and oxidized, reducing the solution pH and leading to the dissociation of either bicarbonate ions or carbonic acid into CO_2 (similar to the anode reaction of Scheme 2). A major problem associated

Scheme 2. Reactions Governing Wynveen and Quattrone's Low-Temperature Carbonation Cell

Cathodic Reactions	Anodic Reactions
$O_2 + 2H_2O + 4e^- \rightarrow 4OH^-$	$2H_2 + 4OH^- \rightarrow 4H_2O + 4e^-$
$CO_2 + OH^- \rightarrow HCO_3^-$	$CO_3^{2-} + H_2O \rightarrow HCO_3^- + OH^-$
$HCO_3^- + OH^- \rightarrow CO_3^{2-} + H_2O$	$HCO_3^- \rightarrow CO_2 + OH^-$

with this system was the poor ionic selectivity of the electrolyte-imbibed porous matrix used to separate the electrodes. The architecture was more recently improved by Eisaman *et al.* by the use of anion exchange membranes,[46] but the current density of the CO_2 concentrator was low (0.5 mA cm^{-2}) and the system required a particularly high humidity in order to prevent electrolyte precipitation. Additionally, the energy required to run the process was 350 kJ/mol CO_2 for separation from air, which is significantly higher than the minimum separation work, yielding low energetic efficiencies.

Early work for eCCC also considered operating carbonation cells under high temperature conditions. These approaches essentially adapted molten carbonate fuel cell platforms for carbon capture and concentration (i.e., driven mode), with some methods also using schemes that can generate energy simultaneously (i.e., fuel-cell mode). Compared to the low temperature carbonation cells, which use aqueous-based electrolytes, these devices employ molten salt electrolytes. This enables lower sensitivity to feed-gas humidity, higher conductivity, and in previous demonstrations, allowed for higher current densities with either similar or improved system efficiencies. The higher temperatures also improve electrode kinetics, which can reduce the need for noble metal catalysts.[47,48] The reaction mechanisms are similar to those described for low-temperature carbonation cells, where CO_2 is consumed at the cathode and discharged at the anode, but the cells are run at much higher temperatures (≥500 °C). Kang and Winnick demonstrated a molten carbonate CO_2 capture device in a driven mode, where CO_2 was concentrated from 1% to 5.8% and 0.25% to 3.4% in a lab-scale cell.[49] The low CO_2 concentration at the anode was due to use of a nitrogen (N_2) sweep gas to collect the released CO_2, therefore, it is expected that the level of CO_2 concentration at the anode will be higher in a more optimized and scaled up device. However, similar to low temperature devices, this type of cell is limited in its ability to recover CO_2 at high purities due to the simultaneous production of O_2 at the anode (as described in Scheme 1).

2.2. Current eCCC Approaches

Since Huebscher and Babinsky's system in 1969, the eCCC field has expanded due to the increasing urgency for global decarbonatization. This has included the addition of new eCCC methods that can be broadly categorized into three different capture approaches: (1) pH-mediated systems, (2) electrochemically mediated amine regeneration (EMAR), and (3) methods involving redox-active capture molecules.

(1) The first approach, pH-mediated systems, use electrochemical reactions to change the pH of an aqueous electrolyte or within an ion exchange membrane. The increase or decrease in pH drives carbonation reactions, leading to CO_2 capture or release, respectively. The carbonation cell technologies described in section 2.1 can be generally categorized as a pH-mediated approach. In more recent work, bipolar membrane electrodialysis was employed for pH-mediated eCCC, where Eisaman *et al.* demonstrated one of the earliest examples in 2011.[50] Watkins *et al.* introduced another approach in 2015, where redox mediators that undergo proton coupled electron transfer (PCET) reactions are used to alter the solution pH for CO_2 capture/release.[51] Many of the pH-mediated systems are further discussed in section 3, with an emphasis on those that use PCET mediators.

(2) The second method, electrochemically mediated amine regeneration (EMAR), was introduced by Stern *et al.* in 2013.[35] Similar to thermally driven postcombustion capture approaches, their system uses amines to capture CO_2. However, an electrochemical reactor drives CO_2 release by specifically oxidizing/dissolving copper which preferentially binds to the amine over CO_2. Section 4 further describes the EMAR approach and relevant literature.

https://doi.org/10.1021/acs.chemrev.2c00681
Chem. Rev. 2023, 123, 8069−8098

(3) The third approach employs redox-active molecules capable of directly binding/releasing CO_2 following changes in oxidation. DuBois and co-workers published the first report of using redox-active capture molecules for eCCC in 1988.[52] In this NASA-funded study, they identified quinones and transition metal complexes as capable of electrochemical pumping of CO_2. Just one year later, Mizen and Wrighton published their report on the CO_2 binding capability of 9,10-phenanthrenequinone in eCCC systems. These publications led to further study of many other quinones as well as other types of redox-active capture molecules from the 1990s through today, and this progress is discussed further in section 5.

2.3. Metrics for Evaluating eCCC

Development of consensus around key performance metrics and associated approaches to evaluating and reporting those metrics is important to continuing the advancement of the eCCC field, enabling comparisons between disparate approaches, highlighting technical progress, and clarifying common challenges. Such metrics are yet to be agreed upon, perhaps due to the size of and state-of-knowledge in this nascent community, but we anticipate such practices will evolve as the field grows. Here we briefly review a few important performance indicators that are currently used to assess carbon capture systems, and more specifically eCCC-based devices, which we refer to throughout this review. For the CCC field in general, the ***capture efficiency*** or ***capture fraction*** is used to describe the percent or fraction of CO_2 that is removed from the feed gas. This is especially important for postcombustion capture technologies, where the objective is to remove most of the CO_2. Additionally, as energy use is a major cost driver for carbon capture systems, ***energy requirements*** are a commonly reported metric. The requirements are often normalized to an amount of CO_2 separated (i.e., units of kJ/mol CO_2) and can also be compared to the thermodynamic minima as a measure of ***energetic efficiency***. For most, if not all, envisioned eCCC systems, the main energy consumer is the electrochemical cell, where the total energy used can be computed from the cell voltage (units of V or J C^{-1}) and charge passed (Q, units of C) as $\int V_{cell}\, dQ$. Again, this is usually normalized by the measured quantity of CO_2 separated. While energy requirements or energetic efficiency may allow for quantitative comparisons between eCCC approaches, care should be taken when expanding such analyses to include approaches which leverage different forms of energy. For example, state-of-the-art amine scrubbing processes for postcombustion capture typically require ≥100 kJ/mol CO_2,[20−23,28] but differences in the quality and cost of heat and electrical work preclude direct comparison. An alternate method, which can allow broader assessments, is the comparison of exergy requirements or efficiency, rather than energy use.[53,54]

Another important metric is the ***Faradaic efficiency***, which, for eCCC, is defined as the actual moles of CO_2 separated per moles of electron transferred. This value may be normalized to the theoretical moles of CO_2 separated per moles of electron transferred (based on stoichiometry) such that it scales from 0 to 1 (or 0−100% as a percentage). This measure provides insight into the selectivity of the capture media and effectiveness of the overall system in using electrical current to drive CO_2 capture/release. Deviations from the stoichiometric maximum of Faradaic efficiency may occur due to factors such as inadequate mediator/sorbent properties (e.g., weak binding affinities), relatively high CO_2 solubility (relative to mediator concentration/quantity), or parasitic side reactions. The **CO_2 *separation capacity*** is another important metric for CCC in general, which represents the total quantity of CO_2 captured/released (moles or mass). Similar to the Faradaic efficiency, this metric can be compared to the theoretical amount to indicate whether side reactions or other factors are limiting performance. For either the Faradaic efficiency or CO_2 separation capacity metrics described above, collecting data over a period of time or many reduction/oxidation cycles is important, as it will indicate system stability over relevant time scales. We also note that eCCC literature may also assess stability of redox mediator by presenting capacity (in terms of total charge passed to the mediator) over many cycles.

While, to the best of our knowledge, there is no agreed-upon standard at the time of writing, metrics that indicate ***specific capacity*** (for CO_2 separation) are also important as this directly correlates with material costs. For liquid-based mediators, specific capacity may be reported in terms of a volumetric concentration (e.g., moles of CO_2 per liter of electrolyte). If the specific capacity is not reported, the volumetric concentration or solubility of the redox mediator and/or sorbent is commonly provided, which can be used to compute theoretical CO_2 separation capacity according to reaction stoichiometry. For solid mediators, which are typically immobilized on an electrode surface, specific capacity may be reported as quantity of CO_2 that was (or could be) captured per electrode area. We note that this metric may also be reported for liquid-based mediators implemented in gas-fed electrochemical reactors. Specific capacity for solid mediators may also be described as CO_2 quantity per mass of redox mediator. Both presentations will be important regarding material costs, as these will indicate the total cell area and mediator/sorbent requirements.

Finally, cell performance indicators, such as ***cell voltage*** (units of V or J C^{-1}) and ***current density*** (units of A m^{-2} or C s^{-1} m^{-2}) are also important and commonly cited. For example, an eCCC device that operates at higher current densities will require less area to separate a given quantity of CO_2, reducing the material needs and system footprint. However, driving the process at these rates may require increased overpotentials and overall cell voltage, leading to higher energy requirements and sacrificing energetic efficiency. Other relevant cell properties may also be reported, including the ohmic resistance of the membrane/separator (due to its influence on the voltage−current density relationship) and the operating conversion rate of the electrochemical cell (which will impact system material requirements and costs). Additionally, there are critical material/molecular properties particular to each type of system that will be described in Sections 3−5.

3. PH-MEDIATED ECCC SYSTEMS

3.1. Overview

Electrochemically generated pH changes in aqueous solutions present a particularly unique approach for the absorption and release of carbon dioxide. Like other solvents, the concentration of physically dissolved CO_2 in water remains constant at a given temperature and pressure in accordance with Henry's law. Unlike other solvents, however, water readily reacts with dissolved CO_2 in solution to form a complex buffer

https://doi.org/10.1021/acs.chemrev.2c00681
Chem. Rev. 2023, 123, 8069−8098

consisting of carbonic acid, bicarbonate, and carbonate (eq 3−5).

$$CO_{2(aq)} + H_2O \overset{K_1}{\leftrightarrow} H_2CO_3 \quad (3)$$

$$H_2CO_3 + OH^- \overset{K_2}{\leftrightarrow} HCO_3^- + H_2O \quad (4)$$

$$HCO_3^- + OH^- \overset{K_3}{\leftrightarrow} CO_3^{2-} + H_2O \quad (5)$$

The concentration and proportion of these species is dependent upon the solution pH. At high pH, the reactivity of CO_2 with hydroxide results in a larger concentration of CO_2 effectively "stored" in solution in the form of carbonate or bicarbonate. Acidification of the solution reverses the buffer equilibrium and releases the captured gas. Recently, research groups have sought to exploit this characteristic of aqueous systems for the development of electrochemical CCC systems. Here, we provide a short overview of electrodialysis/electrodeionization systems and more extensively describe pH-swings with redox mediators. A more thorough description of electrodialysis/electrodeionization is provided in the recent review by Sharifian *et al.*[55]

3.1.1. Electrodialysis/Electrodeionization. Bipolar membrane electrodialysis (BPMED) has been applied as one method for pH-mediated eCCC.[56] BPMED uses electrical current and a combination of cation exchange, anion exchange, and/or bipolar membranes to separate a solution by charge. In aqueous media, the water molecules are split into protons and hydroxide ions to balance charge. Thus, using a sodium chloride (NaCl) electrolyte, the electrolyte separates into sodium hydroxide (NaOH) and hydrochloric acid (HCl). In the capture stage, CO_2 reacts with NaOH to form sodium carbonate. The process can be reversed to release CO_2.

BPMED has been studied for a variety of carbon capture applications. For direct air capture (~400 ppm of CO_2), Eisaman *et al.* found that when using solutions of sodium or potassium hydroxide and applying a constant-current across a BPMED stack, it is possible to remove CO_2 with an energetic cost of about 200 kJ/mol CO_2; the regeneration of CO_2 using BPMED from carbonate requires an additional ~100 kJ/mol CO_2.[50,57] Therefore, the entire process requires an energy input of ~300 kJ/mol CO_2 to extract and recover carbon dioxide from the atmosphere. Sabatino *et al.* noted in their techno-economic review that their direct air capture setup has an energy requirement as low as 236 kJ/mol CO_2, but would cost ≥$773/ton CO_2 due to the high costs of bipolar and ion exchange membranes.[58] For postcombustion capture applications, Carlson and co-workers employed a combination of BPMED and electrodeionization in their process.[59] This system effectively modulated the solution pH, capturing up to 80% of the CO_2 from a simulated flue gas (15% CO_2, balance N_2) and recovering it at high purities (>98% CO_2). However, energy requirements of this system were not reported.

BPMED was also used to remove CO_2 from seawater, samples were run through a BPMED system to separate them into acidified and basified seawater solutions. The minimum total electrochemical energetic input for extracting 59% of the total CO_2 in solution was 242 kJ/mol, which was expected to improve with the scale-up of the BPMED to commercial-scale seawater capture systems.[60] Additionally, Carlson and co-workers attempted to capture CO_2 from flue gas using a combination of BPMED and electrodeionization.[59] This system effectively modulated the solution pH, and CO_2 was concentrated to an 80% CO_2 stream from a 15% inlet stream. Later work by Digdaya *et al.* improved the capture efficiency to extract 71% of the total CO_2 in solution and reduced the electrochemical energy requirements to 155 kJ/mol by changing the redox mediator.[61]

3.1.2. pH-Swing with PCET Mediators. Other systems capitalize on pH changes by using redox-active proton mediators. Compounds capable of proton coupled electron transfer (PCET) have the potential to be particularly useful for pH-swing eCCC processes, which utilize an electrochemical bias to shift pH in one direction or the other to facilitate CO_2 capture or release. In a typical system, a CO_2-containing feed stream is contacted with a basic solution and captured in the form of dissolved inorganic carbon (HCO_3^-, CO_3^{2-}, and $CO_{2(aq)}$). To release the captured gas, a potential is applied (E_{app1}, Figure 2) to oxidize the mediator, which consequently undergoes deprotonation. Acidification due to mediator deprotonation shifts the equilibrium to favor CO_2 evolution. To regenerate the basic solution, a more negative potential (E_{app2}, Figure 2) is applied to reduce, and consequently protonate, the mediator. The resulting increase in solution basicity promotes CO_2 capture *via* dissolved inorganic carbon formation, completing the overall cycle.

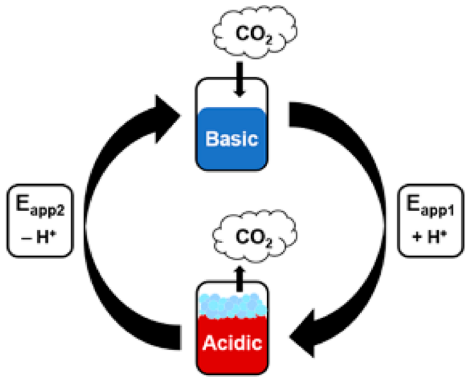

Figure 2. General representation of a pH mediated eCCC cycle.

For efficient CO_2 separation *via* pH-swing eCCC, an ideal PCET redox mediator should be highly soluble and have a sufficiently high pK_a difference in its reduced/oxidized forms to generate large pH changes adequate for CO_2 capture and release. The mediator must also be stable and have sufficient solubility under both acidic and alkaline conditions for extended periods of time. Additionally, these molecules must exhibit stability in the presence of the feed gas composition of interest. For example, air contains high concentrations of oxygen, and thus the mediator must be O_2-stable in these DAC applications. Lastly, mediators capable of concerted proton−electron transfer (CPET) reactions are beneficial as they can enable operation at milder potentials.[62] Several classes of molecules have been identified as candidate redox mediators for pH-swing driven eCCC, including quinones,[51,63−69] phenazines,[70−72] redox-active amines,[73] inorganic compounds,[74,75] and even a riboflavin compound.[76]

3.2. Demonstrations

3.2.1. Quinones. Quinones are a well-studied family of molecules that have been shown to readily undergo 2 H^+, 2 e^- PCET reactions to interconvert between their quinone and hydroquinone forms (Scheme 3).[77,78] Reduced quinones have

https://doi.org/10.1021/acs.chemrev.2c00681
Chem. Rev. 2023, 123, 8069−8098

Scheme 3. Quinones Can Undergo Two Separate One-Electron Reductions in the Presence of a Proton Source to Form the Semiquinone (SQ) and the Hydroquinone (HQ)

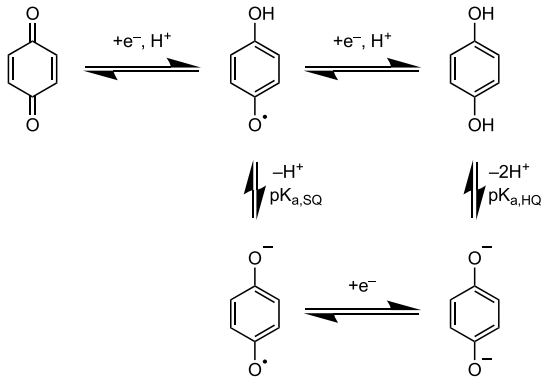

also been used to directly capture CO_2 in aprotic conditions, as described in section 5. However, in protic conditions such as water, formation of the hydroquinone is sometimes more favorable over the CO_2-bound species. The corresponding base (hydroxide if water is the proton source) can also capture CO_2. In this section, their use in pH-swing cycles will be discussed. The ubiquity of quinones in nature and other fields of research has led to a large catalogue of commercially available or readily accessible derivatives that span an extensive range of measured redox potentials and solubilities.[63−65] Additionally, many quinones undergo PCET reactions in aqueous solutions with facile conversion between quinone and hydroquinone forms.[77] Unfortunately, most commercially available quinones have limited solubility and stability in aqueous solutions, confining the current landscape of suitable candidates to only a handful of examples.[66−68] However, these types of properties can be improved with molecular functionalization.[69] Huang *et al.* reported the utilization of tiron (disodium 4,5-dihydroxy-1,3-benzenedisulfonate, an *ortho*-hydroquinone) as a redox-active pH mediator to successfully capture and release carbon dioxide from simulated flue gas (12% CO_2) streams.[64] In a proof-of-concept demonstration with 0.7 M quinone concentration in solution, the pH was changed between 9.2 and 5.7 using constant current electrolysis at 18 mA cm^{-2}. The system was generally effective, operating at >90% Faradaic efficiency, and the estimated energy requirements were similar to existing thermally driven systems (2.4 GJ/metric ton CO_2 or 105.6 kJ/mol CO_2). However, a N_2 sweep gas was used in this demonstration to remove desorbed CO_2, which is not representative of expected system operation where CO_2 is collected at high concentrations. Thus, energetic and Faradaic efficiencies are expected to be lower than these reported values under more realistic operating conditions. Despite this, the experiment was run in a nonoptimized H-cell platform, and performance would be expected to increase as the cell and overall system are engineered for higher performance. Another challenge with this PCET chemistry is its long-term stability: the system was unable to perform multiple capture−release cycles, limiting its practicality.

Watkins *et al.* explored a different system, where 2,6-dimethylbenzoquinone was used as the pH mediator of choice and was employed in a gas-fed electrolyzer.[51] In their system, a porous separator was soaked in the liquid electrolyte solution containing 10 mM 2,6-dimethylbenzoquinone and 10 mM of the equivalent corresponding hydroquinone and supported between two gas diffusion electrodes (depicted in Figure 3). In their system, the liquid electrolyte saturated separator works in

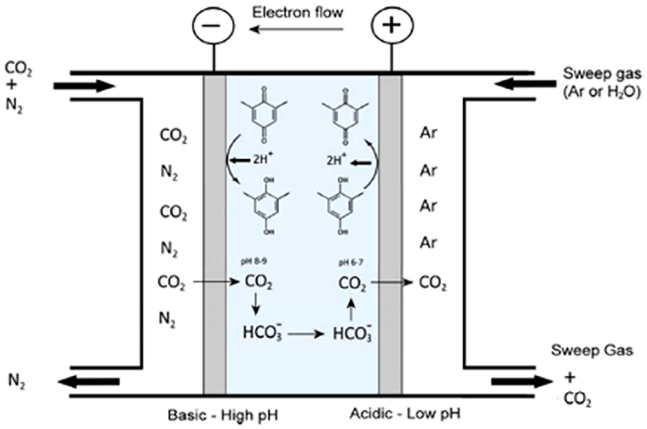

Figure 3. General representation of a membrane-supported polymer system developed by Watkins *et al.* in ref 51. Reproduced with permission from the American Chemical Society.

conjunction with metal catalyst-coated electrodes to effectively drive a pH gradient across the cell. Using platinum (Pt) deposited electrodes, CO_2 was selectively transported from the feed gas side of the cell (cathode) to the collection side of the cell (anode). They demonstrated CO_2 removal at the cathode and recovery at the anode from a simulated flue gas stream (14% CO_2, 3% O_2, and balance N_2) with no transport of other gases detected. Although no energetic efficiencies were reported, large cell voltages were applied (between 1−2.5 V for the Pt catalyst). Jin *et al.* estimated that the required energy of this experimental demonstration was ∼600 kJ/mol CO_2.[79] Additionally, low quinone solubility limited the operating concentrations, thus preventing the large pH swings that are required for high CO_2 removal efficiency.

3.2.2. Phenazines. Phenazines are another promising family of redox-active pH-mediator compounds. Analogous to quinones, phenazines reversibly undergo 2H$^+$, 2e$^-$ PCET reactions over a wide pH range. Sulfonated phenazine derivatives have also displayed high aqueous solution solubilities and stabilities. Jin *et al.* demonstrated use of 3,3′-(phenazine-2,3-diylbis(oxy))bis(propane-1-sulfonate) in a pH-swing system for carbon capture.[70] In the absence of CO_2, the pH was increased from 4 to 13.4 using 0.1 M phenazine concentration, and then cycled between a pH of 13.4 and 7.5 over four total cycles. When a continuous flowing stream of a CO_2/N_2 mixture (CO_2 partial pressure of 0.465 bar or 46.5% CO_2 and balance N_2) was contacted with the electrolyte, they observed a decrease in CO_2 partial pressure down to ca. 0.38 bar following deacidificiation and an increase up to ca. 0.57 bar following acidification. During the desorption step, a 100% CO_2 stream was used to simulate more realistic operating conditions, where CO_2 must be released and concentrated to high purities. For their system setup, Jin *et al.* estimated from thermodynamic calculations that a minimum of 16−75 and 30−75 kJ/mol CO_2 is required for capture from 10% and atmospheric CO_2 sources, respectively (which corresponds to 8−35% and 27−67% energetic efficiency compared to the theoretical capture limits of 5.7 and 19.4 kJ/mol CO_2 described in section 1). Comparatively, experimental data indicate that their system can separate carbon dioxide from a mixture containing 46.5% CO_2 with energy requirements in

https://doi.org/10.1021/acs.chemrev.2c00681
Chem. Rev. 2023, 123, 8069−8098

the range of 49−120 kJ/mol CO_2, depending on the operating current density (which corresponds to an energetic efficiency of ∼2−4% based on a theoretical minimum of 1.9 kJ/mol). One limitation of this system, and pH-mediated processes for eCCC in general, is slow CO_2 absorption kinetics. In their specific demonstration, CO_2 absorption had to be continued for roughly 40 min after completion of electrochemical deacidification.

In another study, Xie *et al.* utilized a series of phenazine PCET pH-mediators in a continuous flow eCCC setup (Figure 4).[71] They identified 7,8-dihydroxyphenazine-2-sulfonic acid as

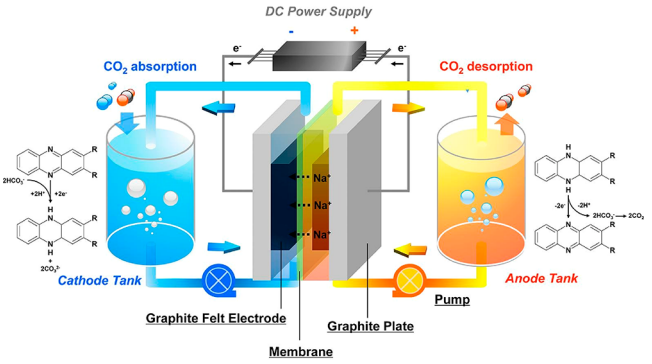

Figure 4. Continuous flow eCCC system featuring phenazine PCET pH-mediators reported by Xie *et al.* Reproduced with permission from ref 71. Copyright 2020 Elsevier.

the most effective phenazine derivative. Using a 25 mM phenazine concentration, capture from a simulated flue gas composition (15:85 CO_2:N_2) with an estimated energy consumption of 0.49 GJ/metric ton CO_2 (22 kJ/mol), and Faradaic efficiency >95% was performed. Their estimated energetic efficiencies are highly competitive with other CCC approaches, surpassing state-of-the-art amine capture systems (estimated at 21% using 4.7 kJ/mol CO_2 as the theoretical minimum required).[24,25] However, CO_2 release during desorption was measured using a N_2 or argon (Ar) carrier gas, which is not representative of a real system where carbon dioxide is released and concentrated to high CO_2 concentrations. Thus, energy requirements will likely be higher and Faradaic efficiencies will be lower than reported values in the study. Their system displayed high stability in the presence of CO_2 and N_2 over the tested time-scale; Xie *et al.* estimated a capacity retention of 97.9% over eight capture−release cycles. Despite these findings, they anticipate that this phenazine compound may be O_2-sensitive, which could significantly reduce its effective stability under practical conditions.

The same group (Xie *et al.*) later demonstrated the use of the proton-carrier riboflavin 5′-monophosphate sodium salt hydrate at a concentration of 25 mM in aqueous solution as a PCET pH-mediator in these types of systems.[76] In a similar setup, they demonstrated CO_2 capture from a 15:85 CO_2:N_2 flue gas stream, with estimated energy requirements of 9.8 kJ/mol CO_2 (which corresponds to a 48% efficiency) and Faradaic efficiencies of >93%. Similar to their previous study, they used a carrier gas (N_2 or Ar) during desorption. Therefore, expected energy requirements and Faradaic efficiency under more practical operation is currently unclear for this system. This chemistry exhibited relatively good stability in the N_2/CO_2 environment, with 0.39% capacity fade per cycle measured over 21 total cycles; however, O_2 stability was not reported. One current limitation of this riboflavin derivative is its low solubility (25 mM compared to ≤1 M for quinones[80]), which limits redox-mediator concentration and thus both the pH swing and ultimately CO_2 separation capacity.

More recently, Aziz and co-workers utilized a sulfonated phenazine derivative (DSPZ, Figure 5) as a PCET pH-mediator.[72] Using an aqueous solution containing 110 mM DSPZ, they were able to capture and concentrate CO_2 from 0.1 bar (10% CO_2 with N_2 balance) to 1 bar (100%), with a pH swing of ∼4 units per cycle (pH varied between 6 and 10). An estimated 61.3 kJ/mol CO_2 is required to achieve concentration from 10 to 100% (corresponding to ∼9% energetic efficiency based on the theoretical limit calculated in section 1) when operating at 20 mA/cm^2. When extrapolated for DAC applications, the authors estimate a work requirement of ∼121−237 kJ/mol CO_2 when operating at the same current

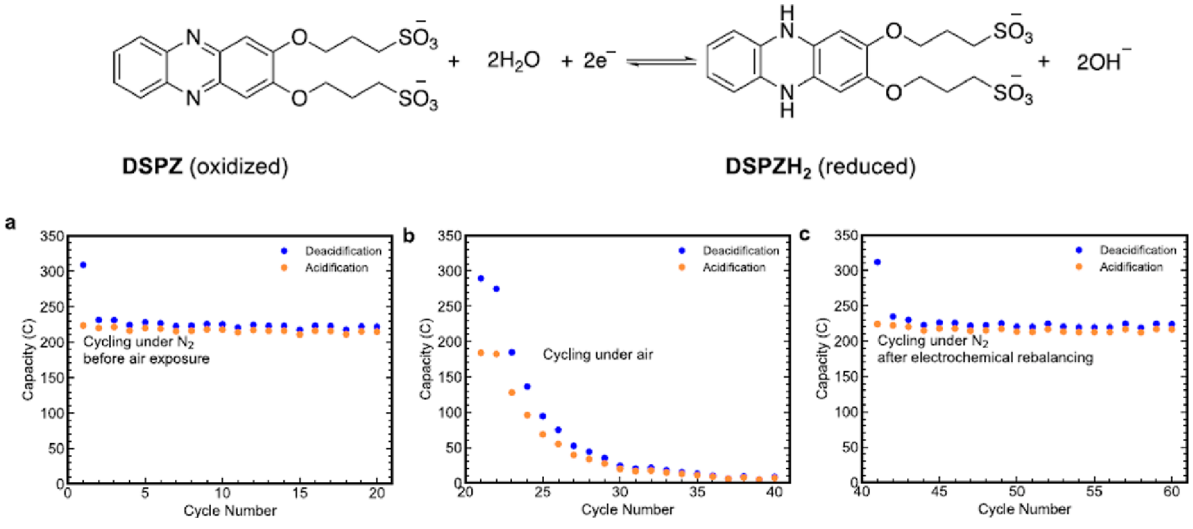

Figure 5. Phenazine PCET pH mediator reported by Jin *et al.*, and capacity data over many cycles obtained in their continuous flow eCCC system under (a) N_2 and (b) air environments. (c) Cycling data in a N_2 environment after employing their "electrochemical rebalancing" technique following the capacity fade in air. Reproduced with permission from ref 72. Copyright 2022 Nature.

https://doi.org/10.1021/acs.chemrev.2c00681
Chem. Rev. 2023, 123, 8069−8098

density (8−16% energetic efficiency compared to theoretical limit of 19.4 kJ/mol CO_2). The system is quite robust, showing little to no loss in capture capacity after 20+ cycles (Figure 5a). Their PCET chemistry does show significant O_2 sensitivity, however, with a 65% drop in capacity after the first cycle and nearly complete capacity loss by the 20th cycle in the presence of O_2 (Figure 5b). What is of particular interest in this work is the utilization of "electrochemical rebalancing" to offset this loss in capacity due to O_2. In the utilized "electrochemical rebalancing", off-cycle deactivated species in solution are electrochemically converted back to their active state. After electrochemical rebalancing, the authors show regeneration of the solution to original capacity levels (Figure 5c).

3.2.3. Redox-Active Amine. Hatton and co-workers investigated a system that uses a redox-active amine for capture *via* pH swing.[73] Cationic 1-aminopyridinium nitrate was identified as a redox-active pH mediator as it has a reversible redox couple in water (1-aminopyridinium cation/1-aminopyridinyl radical). An aqueous 0.2 M 1-aminopyridinyl solution was reduced in the presence of N_2, then exposed to 100% CO_2. Full conversion to the radical had a 53% Faradaic efficiency with an estimated minimum energy consumption of 101 kJ/mol CO_2. The authors projected that partial regeneration of the amine may enable lower energy requirements (in the range of 40−80 kJ/mol CO_2). Notably, they studied the stability of the radical in an oxygenated atmosphere over a period of one month. The radical was not stable over long periods of time, leading to capacity decreases of 6.6% and 46% over 1 and 30 days, respectively. However, they also studied the radical in a N_2 atmosphere and found that after 30 days, the capacity decreased to 55%. The authors conjecture that the radical may be reacting with itself to form 4,4′-bipyridine.

3.2.4. Inorganic Compounds. In a different approach, Rahimi *et al.* proposed using manganese oxide (MnO_2) coated electrodes to act as heterogeneous PCET pH-mediators, according to eq 6, to generate pH-swings and therefore drive CO_2 capture.[75]

$$MnO_{2(s)} + H^+ + e^- \rightleftharpoons MnOOH_{(s)} \quad (6)$$

One benefit to this system is that manganese oxides and hydroxides (MnOOH) are highly stable at various pH values and MnO_2 readily undergoes PCET reactions in aqueous solutions.[74] In Rahimi *et al.*'s system, the pH mediator is immobilized on the electrode surface, which requires batch-type operation where the electrode polarity must be switched periodically to drive CO_2 capture and release *via* proton intercalation and deintercalation of the electrodes, respectively. In their bench-scale demonstration, a cell voltage of 1 V was applied, and polarity was switched every 2 h for a total of 4 cycles (i.e., 8 h), where ∼0.4 mmol of CO_2 was captured and recovered each cycle.[81] Energy requirements were not reported; however, in their earlier study, Rahimi *et al.* used a simple modeling approach (i.e., thermodynamic cycle analysis with overpotential prediction) to estimate that this pH-swing process could theoretically separate CO_2 from flue gas (15% CO_2) at an energetic cost of 33.2 kJ/mol CO_2 (∼14% energetic efficiency using a theoretical minimum requirement of 4.7 kJ/mol).[75]

3.3. Cell and System Design

Current studies involving pH swings (and eCCC systems in general) mainly include proof-of-concept demonstrations with candidate chemistries that are important in early stage research. However, there is less research involving characterization of cell performance and optimization of experimental configurations. Transitioning toward higher performance pH-swing eCCC systems will require not only optimized redox mediator molecules, but also engineered cell/system designs that maximize CO_2 separation capacity and simultaneously minimize energy losses associated with kinetics, ohmics, and mass transport. This will be impacted by several factors, including solubility/concentration of the pH mediator and CO_2 sorbent (or electrode capacity for immobilized mediators) as well as properties impacting kinetics, mass transport, and ohmics. While Liu *et al.* discuss such aspects of system design in more detail (particularly for continuous flow systems),[82] here we focus on reviewing current experimental cell designs for pH-swing approaches. We aim to contextualize where the field is at in terms of cell/system design, provide important cell performance/operation metrics, and highlight key challenges with these systems to inspire future work.

A common experimental setup employed for pH-swing systems resembles a redox-flow battery (RFB) (shown in Figure 4). Both Xie *et al.* and Jin *et al.* used this type of setup to test their phenazine and riboflavin chemistries, as previously described.[70−72,76] This type of system is comprised of a flow cell, two reservoir tanks to contain the positive, and negative electrolytes (typically 7−50 mL), respectively, and pumps to circulate the working and counter electrolytes through the cell (Jin *et al.* and Xie *et al.* reported using electrolyte flow rates of 100 and 200 mL min^{-1}, respectively). The cell design employs porous carbon electrodes (typically paper, cloth, or felt) and engineered flow fields to deliver the electrolyte solution to the electrode. A membrane or separator is used to physically separate the two electrodes while enabling ions (e.g., Na^+ or K^+) to exchange between the electrolytes to maintain electroneutrality. This setup operates in a cyclic fashion (charge/discharge cycles), applying a current or cell voltage to deprotonate the mediator, then switching the direction of current flow or electrode polarity to protonate the mediator. CO_2-containing feed gas (or sweep gas) is then contacted with the liquid electrolyte in the working-side reservoir during and/or after the protonation (or deprotonation) half-cycle to enable CO_2 capture (or removal). Xie *et al.* used 4 cm^2 (geometric/projected area) graphite felt electrodes, serpentine or flow-through flow fields, and a Nafion 115 or 117 cation exchange membrane in their experiments.[71,76] Their cell was operated with applied current densities of 10−30 mA cm^{-2}, resulting in average cell voltages of ca. 0.06−0.2 V. While these low voltages led to low energy requirements, the experimental system requires validation with a pure CO_2 sweep gas at the anode to understand performance under more realistic operating conditions. Additionally, a key engineering challenge for this cell setup in its current form is a relatively high ohmic resistance (2.48 Ω or 9.92 Ω cm^{-2} measured with EIS), which may induce large energetic penalties and/or limit achievable current densities.[71] Jin *et al.* reported a flow cell consisting of a Fumatech cation exchange membrane (E-620(K)), serpentine flow fields, and 5 cm^2 SGL 39AA porous carbon paper electrodes (pretreated in air at 400 °C for 24 h).[70,72] The cell was operated galvanostatically at current densities of 20−150 cm^{-2} with potential holds at the end of each half-cycle. As expected, high cell voltages were reported as current density was increased. However, dominant sources of cell over-

https://doi.org/10.1021/acs.chemrev.2c00681
Chem. Rev. 2023, 123, 8069−8098

potentials, and other challenges limiting performance, were not directly discussed.

Watkins *et al.* employed a different cell configuration, similar to a fuel cell, to test solubilized quinone mediators.[51] The system utilized a gas-fed electrochemical reactor (shown in Figure 3 above) which could operate in a continuous fashion. As described previously, the cell contained catalyst-coated gas diffusion electrodes and an electrolyte imbibed separator. Their electrodes consisted of Sigracet 25 BC carbon paper with a hydrophobized microporous layer (MPL), and they applied a catalyst layer on top of the MPL. Their separator was a hydrophilic porous polypropylene material (Celgard 3501) that was soaked in liquid electrolyte before assembling and running the cell. The liquid electrolyte was an aqueous solution consisting of 10 mM of the quinone, 10 mM of the hydroquinone, and 1 M $NaHCO_3$ which served as both the sorbent and supporting salt. Flow fields (25 cm^2) were employed to distribute and remove gases to and from the electrodes. Gases that were fed to their system on the capture (cathode) and release (anode) sides were prehumidified, which is typically done in low-temperature fuel-cell technologies to prevent the membrane/separator from drying out. Watson *et al.* explored the use of platinum, palladium, and ruthenium catalysts, and found that platinum enabled the greatest CO_2 concentration change and suppressed water splitting across a range of cell potentials (1−2.5 V). Cell voltage requirements were high for this system compared to the approaches mentioned above, without a clear understanding of what phenomena contributed to this inefficiency (e.g., ohmic overpotentials from the membrane, contact resistances, kinetic overpotentials due to slow electrochemical reactions, etc.).

As previously described, the MnO_2-based technology of Rahimi *et al.* makes use of solid rather than solubilized pH mediators. They specifically immobilized MnO_2 onto carbon cloth electrodes, where they tested two fabrication methods. The first was a casting method, where MnO_2 powder was synthesized using coprecipitation, and then a slurry containing this active species was cast onto a carbon-based, porous substrate. The second method involved electrodeposition of MnO_2 onto the substrate, which was shown to achieve more uniform deposition and higher capacitance (specific and geometric). To test their electrodes, they used a liquid flow-based setup to test their MnO_2 mediator system. The platform was similar to the RFB-type systems described above, consisting of an electrochemical cell to drive protonation/deprotonation, reservoir tanks to hold liquid electrolyte for the working and counter sides of the cell, and pumps to circulate electrolyte between the cell and reservoirs. Their liquid-fed cell consisted of 25.8 cm^2 carbon cloth electrodes (AvCarb) coated with MnO_2 particles, parallel flow channels to deliver electrolyte to the electrodes, and a Selemion AMV anion exchange membrane. The flow channels also contained plastic baffles (a form of turbulence promoters) to enhance mass transport by specifically disrupting boundary layer growth, preventing channeling, and increasing local velocity.[83] Due to the use of redox mediators immobilized on the electrode surface, the cell must be operated in a batch mode, where polarity is switched in cycles to prevent the complete proton saturation and depletion of the electrodes, respectively. In this study, the cell adopted a symmetric format with identical electrodes on either side, and the experiments were also started with the same electrolyte concentrations. During each half-cycle, the cell was operated with a constant applied potential of ±1 V, while the measured current density varied within the range of ±0−2 mA cm^{-2}. Absorption or desorption of CO_2 was carried out in a separate step following each electrolysis half-cycle by contacting the electrolyte with the feed or sweep gas. Overall, the cell was limited to low current densities and energy requirements were not reported; therefore, cell characterization and optimization work would be beneficial.

4. ELECTROCHEMICALLY MEDIATED AMINE REGENERATION (EMAR)

4.1. Overview

As previously described, one of the most investigated methods for CO_2 capture from power plant flue gas uses amine absorbents. The standard amine used for this method is monoethanolamine (MEA) because it has a high rate of CO_2 absorption, easy regeneration, and low replacement cost.[84] In this process, the flue gas is brought into contact with the amine solution in an absorber, where the amine effectively captures CO_2 to form a carbamate. The carbamate solution is heated (~110 °C for MEA) in order to break the amine−CO_2 bond,[85] and thus CO_2 is released and collected. However, there are challenges with this traditional regeneration process, including low energetic efficiencies and degradation of amines at high temperatures, suggesting that the operational temperature must be high enough to break the amine−CO_2 bond, but low enough such that the amine does not degrade. Consequently, the temperatures used for the desorption step are not extreme enough to fully liberate the CO_2 bound to amines, as only half of the bound gas is typically released.[86] Additionally, the narrow temperature range decreases the achievable energetic efficiency of the process due to greater Carnot limitations. In order to increase the desorption efficiency, nonthermal methods have been investigated.

Electrochemically mediated amine regeneration (EMAR), developed by Hatton and co-workers, is a promising alternative to temperature swing amine regeneration.[85−87] The EMAR process employs a similar absorption step as the traditional amine-based solvent systems, capitalizing on the affinity of amines for binding CO_2; however, an electrochemical cell is used, rather than a stripping column, to drive CO_2 release (Figure 6). This desorption step specifically relies on the use of an electrochemically active absorbent blocker (such as copper, Cu) that (1) can be activated *via* oxidation, where it preferentially binds to the amine and therefore displaces captured CO_2, and (2) can be reduced to regenerate both the deactivated blocker and the amine sorbent. Use of an electrochemical cell to drive desorption can potentially liberate up to 80−90% of the absorbed CO_2, an improvement compared to traditional amine-based capture.

The success of EMAR relies on the difference between binding constants of the amine−CO_2 and amine−blocker complex. The amine and blocker should form a stable complex with an equilibrium constant that is much larger than that of the amine with the CO_2. The standard blocker and amine used in EMAR are copper and ethylenediamine (EDA). These species both fit the designated requirements, such that once Cu^{2+} is present in solution the amine will release CO_2 in favor of binding to copper. The reactions and equilibrium constants for EDA with CO_2 and Cu^{2+} are given below (eqs 7 and 8).[85,87]

https://doi.org/10.1021/acs.chemrev.2c00681
Chem. Rev. 2023, 123, 8069−8098

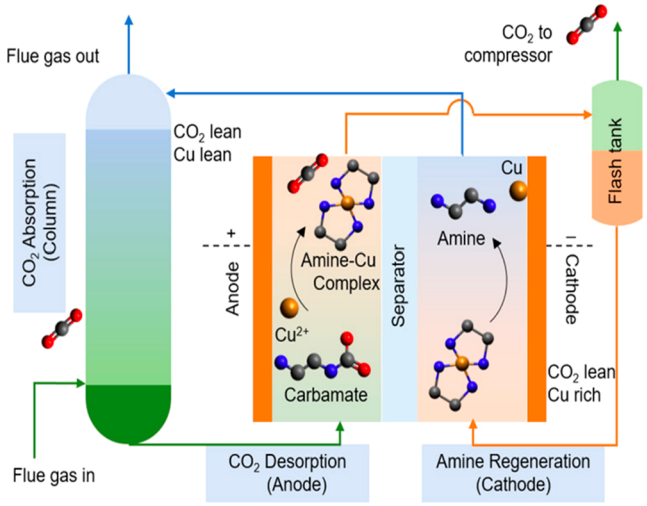

Figure 6. EMAR cycle in which an amine-based solvent is brought into contact with simulated flue gas in an absorption column, leading to CO_2 capture and carbamate formation. The carbamate-rich amine-based solvent is pumped to the anodic compartment. Upon electrochemical oxidation, Cu^{2+} is introduced to the solution, and the Cu−amine complex forms, releasing CO_2. The gas phase is separated, and the Cu−amine solution is pumped back to the cathodic compartment where Cu^{2+} ions are electrochemically plated onto the electrode, releasing—and, hence, regenerating—the amine. Reproduced with permission from ref 85. Copyright 2020 American Chemical Society.

$$2\mathrm{EDA(aq)} + \mathrm{Cu}^{2+} \overset{K_{\mathrm{Cu}}}{\rightleftharpoons} \mathrm{Cu(EDA)}_2^{2+} \quad (K_{\mathrm{Cu}} = 2.10 \times 10^{18}) \tag{7}$$

$$\mathrm{EDA(aq)} + \mathrm{CO}_2\mathrm{(aq)} \overset{K_{\mathrm{CO}_2}}{\rightleftharpoons} \mathrm{EDA(CO}_2\mathrm{)(aq)} \quad (K_{\mathrm{CO}_2} = 4.90 \times 10^{4}) \tag{8}$$

4.2. Demonstrations

In early work for the EMAR process, Stern *et al.* compared 14 different amines that included monoamines, amino acids, and polyamines before narrowing the selection to just four polyamines: ethylenediamine (EDA), triethylenetetramine (TETA), aminoethylethanolamine (AEEA), and diethylenetriamine (DETA).[35] Polyamines were selected as they are more likely to chelate copper ions with high binding constants to form stable copper complexes. The other 10 amines had a tendency to precipitate as salts, especially in the presence of CO_2, making them unsuitable candidates. The four polyamines were analyzed for their CO_2 loading capacity, copper complexation characteristics, and open-circuit potential measurements. In this study, the CO_2 loading capacity is defined as the total moles of absorbed CO_2 relative to the full capacity of the amines for binding CO_2. In the absence of Cu^{2+}, these four amines have a theoretical CO_2 loading capacity of 0.5 as carbamate formation results in a zwitterion, where two amine functional groups are required for every molecule of captured CO_2 (see section 4.4). However, TETA, AEEA, and DETA all demonstrated loadings below 0.5 (in the range of ∼0.45−0.5), which they theorized to be due to unreacted secondary amine groups that are present in these three polyamines. EDA, which has no secondary amine group, possessed the highest CO_2 loading capacity of slightly over 0.5, which is likely due to the formation of bicarbonate, a common side reaction for primary amines.[86] Stern *et al.* also investigated the amount of copper required to deactivate the amine and they found that for EDA, AEEA, and TETA, one equivalent of Cu^{2+} binds to each amine; however, this ratio for DETA was dependent on the copper loading (which is defined such that it is proportional to Cu^{2+} concentration). At higher copper concentrations, one DETA molecule binds to each Cu^{2+}, and at lower copper loading, two DETA molecules bind to each Cu^{2+}, meaning that more copper is required to deactivate the molecule and release CO_2. Lastly, the difference in open-circuit potential for a copper electrode under anodic and cathodic conditions was used to estimate the minimum energy needed for releasing and removing Cu^{2+} into solution. Under constant amine concentrations, open circuit potentials for a copper electrode were measured for various copper loadings in the presence and absence of CO_2 to represent the anode and cathode, respectively. Minimum work was estimated from these potential differences, which showed relatively similar values for each amine when compared at a 50 °C operating temperature (AEEA = 17.9, EDA = 18.4, TETA = 19.2, DETA = 21.4 kJ/mol CO_2). EDA was also evaluated at 70 °C, where the estimated minimum work decreased to 14.7 kJ/mol CO_2. After these initial tests, EDA was selected as the standard amine for use in EMAR due to its high CO_2 loading capacity, favorable copper complexation in the presence of CO_2, and potential to operate at lower energy requirements under higher temperature operation. EDA has also been identified as a desirable candidate in the thermal-swing CO_2 capture systems; however, the heat required for CO_2 desorption from EDA is too high to be economically practical.[86]

Early bench-scale demonstrations of the EMAR system using EDA-captured CO_2 from a pure feed stream (100%) of CO_2 exhibited an energy requirement of ≤100 kJ/mol CO_2 and Faradaic efficiencies up to 80%.[35,88] Separation from streams with lower CO_2 concentrations were not performed in this early system, as the copper swing of their benchtop system (i.e., conversion between Cu^0 and Cu^{2+} in the electrochemical cell) was not high enough compared to the concentration of CO_2 physically dissolved in solution. Advances in the EMAR cell design have resulted in significant performance improvements, as described in section 4.3. Additionally, more recent EMAR demonstrations have operated at an elevated fluid temperature (55 °C), which enhanced electron transfer kinetics at each electrode and reduce CO_2 solubilities during desorption.[85,89,90] The current bench-scale process can capture CO_2 from a 15% CO_2 feed stream (N_2 balance), while operating at 40−80 kJ/mol CO_2 (which corresponds to ∼6−12% energetic efficiency compared to the theoretical requirement of 4.7 kJ/mol calculated in section 1).[91] The system has also demonstrated stable operation for 50 h.

Liu *et al.* studied the use of MEA rather than EDA in a thermal-electrochemical codriven system (TECS), where they essentially combined the more commonly used amine from thermally driven CO_2 capture and EMAR.[92] This system parallels the EMAR scheme described above (Figure 6), with MEA binding to CO_2 and then Cu^{2+} being introduced electrochemically; however, a thermal step is also used. After Cu^{2+} ions have been stripped and dissolved, the solution is heated to 90 °C to assist in the removal of CO_2 from MEA.[92] The heat was added in TECS to improve the current efficiency and CO_2 desorption yield. Liu et al. discuss how the higher CO_2 desorption yields may have been due to faster copper dissolution, improved CO_2 desorption kinetics, and increased

https://doi.org/10.1021/acs.chemrev.2c00681
Chem. Rev. 2023, 123, 8069−8098

copper concentrations due to the effects of temperature on both the hydrolysis reactions and pH. One challenge they encountered was that the reduction of Cu-MEA, and thus the regeneration of Cu^0 and MEA, was slow. Adjusting Cu^{2+} concentration, CO_2 loading, temperature, and KNO_3 (the supporting salt) concentration of the system improved kinetics and decreased the charge transfer resistance. Further, increasing the Cu^{2+} concentration and temperature improved mass transfer and thus reduced the associated overpotential. A combination of data from experimental techniques (cyclic voltammetry, potentiodynamic polarization, and electrochemical impedance spectroscopy) and a regression analysis found that the optimum operating conditions for this TECS system include Cu^{2+} molality of 0.25 mol kg^{-1}, CO_2 loading of 0.37 mol_{CO2} /mol_{amine}, a temperature of 90 °C, and KNO_3 molality of 1 mol kg^{-1}. Under these conditions, the regeneration energy consumption is predicted to drop to 1.3 GJ/ton CO_2 (63 kJ/mol CO_2).[92] These conditions can enable higher energetic efficiencies than traditional amine regeneration processes, which typically require >2.3 GJ/ton CO_2 (>110 kJ/mol CO_2).[20−23] These efficiencies are also comparable to estimated energy requirements of Wang *et al.* for their lower temperature EMAR system (with EDA) of 40−80 kJ/mol CO_2.[89] However, given the combination of heat and electrical work used to drive these systems, comparison of exergies, rather than energies, may be more indicative of comparative performance.

4.3. Cell and System Design

The EMAR process, pioneered by Hatton and co-workers, is arguably the most developed redox-mediator-based method for eCCC in the peer-reviewed literature, as there have been several benchtop flow-cell level demonstrations, as well as engineering assessments regarding cell design metrics.[35,68,71,82,86−88,91,93] In an early embodiment, the EMAR cell consisted of copper plate electrodes and a porous polypropylene separator (Celgard 3501) to physically separate the cathodic and anodic electrolyte solutions while maintaining an ionic connection. Liquid-phase reactants were fed to the cathode and anode using parallel flow channels with a rectangular cross-section. As described above, early demonstrations with this flow cell captured CO_2 at ≤100 kJ/mol CO_2.[35,88] This prototype cell had a relatively low operating current density (5 mA cm^{-2}) and was limited by low swings in copper loading (i.e., conversions), resulting in less than 1% of bound CO_2 being released per pass in the electrochemical cell.[35,88,93]

Analysis of the EMAR cell using two-dimensional (2D), convection-diffusion modeling of the planar electrodes has suggested large mass transport limitations emerge with increased conversion per pass. Specifically, the model predicts the development of a thick boundary layer in the flow direction, which, in turn, leads to an increase in the cell voltage at relatively low current densities (<8 mA cm^{-2}), where the cell enters a mixed kinetic-mass transfer regime.[93] This limitation can be overcome by increasing the electrolyte flow rates, albeit at the expense of conversion per pass. Wang *et al.* estimate that current densities greater than 50 mA/cm^2 could be achieved with improved mass transport properties of the cell.[89] When tested with galvanostatic experiments (10 mA/cm^2), increasing the flow rate from 75 to 225 mL/min reduced cell voltage by 20%, albeit at the expense of Cu^0/Cu^{2+} conversion per pass and, thus, CO_2 separation capacity. Additionally, large baffles were incorporated into the flow channels of an EMAR cell, which led to a 25% reduction in cell voltage, similar to the effect of increasing flow rate but without decreasing conversion per pass. However, a consequence of such obstructions is increased pressure drop through the cell.[94] More recent generations of EMAR cells have incorporated a pin-type flow channel, with rubber dots arranged in a regular pattern. These cells have exhibited significant performance improvements compared to earlier versions, but it is unclear if and how much the flow channel has contributed to this due to concurrent changes to the cell/system design and operating procedure.[91]

In addition to flow channels, optimization of the electrode geometry will also play a role in improving cell performance. Currently, 2D planar electrodes are used in EMAR. However, in many fields, three-dimensional (3D) porous electrodes have been adopted to enhance performance.[95−97] Overall, these porous electrode structures have a significantly higher reaction area per volume, which permits cell operation at higher geometric current densities with reduced overpotentials compared to planar electrodes.[98] In modeling the EMAR system, Stern *et al.* estimated that a cell with porous electrodes could operate with overpotentials >50% lower than a cell with planar electrodes.[86] When tested, the use of porous copper foam electrodes within the EMAR cell enabled higher Faradaic efficiencies and lower cell resistances; however, performance diminished over a few hours.[93] They believe this failure was due to bubble formation and entrapment within the electrochemical cell. To the best of our knowledge, no further work using porous electrodes within the EMAR cell has been published to date.

Issues associated with plating and stripping copper have also hindered system feasibility and cell performance. During operation, the current density is not uniformly distributed across the electrode leading to spatially varying metal deposition on the cathode and stripping from the anode. Accordingly, authors reported sanding or completely replacing both electrodes between experiments.[93,99] While less of a concern for exploratory studies at the bench-scale, if unaddressed, electrode degradation has the potential to become a significant maintenance challenge during practical implementation. Furthermore, as current density is increased and mass transport limitations emerge, dendritic copper growths can occur during plating. These deposits can become more powder-like as the cell approaches a mass transport controlled regime.[100] In a cell with convective flow, these more loosely bound deposits may be sheared away from the surface,[101] resulting in a permanent loss of copper electrode mass over time. Additionally, dendritic copper growths from the electrode surface can puncture the membrane/separator and come into contact with the opposite electrode, resulting in an internal short circuit.[88] Early EMAR cell designs incorporated a woven cotton cloth (cheesecloth) between the membrane/separator and solid electrode to provide support and prevent this type of contact.[86,88] Use of this material, however, significantly increased the ohmic resistance of the cell. Incorporation of a structured flow field (as described above) not only enhanced mass transport, but also better supported the membrane/separator such that supporting cloth was not required to prevent contact between the electrode and membrane/separator. This arrangement also reduced the ohmic resistance of the cell from 0.6 Ω to 0.0289−0.14 Ω, which led to concomitant decreases in estimated energy requirements for CO_2 separation.[83,88,91] The membrane/separator itself also introduces ohmic losses, which

https://doi.org/10.1021/acs.chemrev.2c00681
Chem. Rev. 2023, 123, 8069−8098

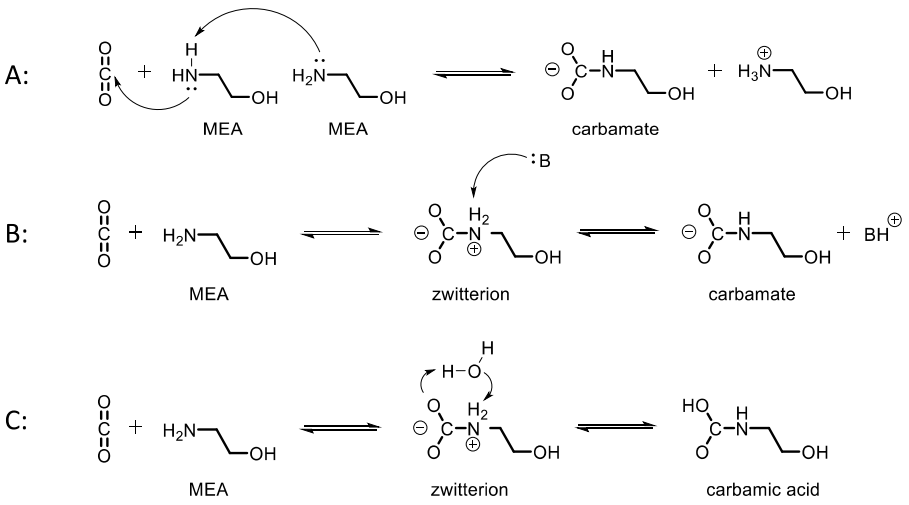

Figure 7. Three suggested reaction mechanisms for CO_2 absorption by MEA: (a) MEA binds one CO_2 molecule and concurrent deprotonation by a second MEA forms a carbamate. (b) MEA binds one CO_2 molecule to form a short-lived zwitterionic intermediate, which is followed by deprotonation by another base (e.g., amine) or solvent to form a carbamate. (c) MEA binds one CO_2 molecule to form a short-lived zwitterionic intermediate, which is followed by a proton transfer from a solvent (water) or amine molecule to form carbamic acid.

depend on membrane/separator class (ion-exchange membrane or porous, nonselective separator) and material. While earlier EMAR demonstrations have mostly used porous, nonselective separators, more recent studies have instead reported using anion-exchange membranes. However, there is no indication of whether this has resulted in performance enhancement.[85,91]

The discussed studies have led to advances in EMAR cell/system design, which have allowed for significant performance improvements. The improved cell platform afforded lower cell overpotentials and thus improved energetics (40−80 kJ/mol CO_2), as well as greater copper loading swings leading to higher regeneration capacities (0.12−0.62 mol CO_2/mol EDA). Despite these advances, cell operation is still limited by relatively low current densities and challenges with copper plating/stripping.

4.4. Computational Insight into Amine/CO_2 Binding

The strength by which a particular amine binds the CO_2 molecule is a decisive factor governing the efficiency of both thermal swing and EMAR technologies. Amines that exhibit stronger CO_2 binding can enable higher removal rates of CO_2 but may require more energy to release CO_2 and regenerate the solvent. However, the seemingly simple process of formation of a carbamate through the reaction of an amine with CO_2 is more complicated due to intermediate reactions following the initial CO_2 uptake. Computational modeling has provided insight into the stability of possible reaction intermediates and energetic barriers for their interconversion and decomposition.[102−104] Modeling has also been used to understand how substituent effects are correlated with binding energies, basicities, or nucleophilicities of the CO_2-binding centers, and also how hydrogen-bonding can influence these trends. However, not all fundamental aspects of CO_2 absorption by amine functionalities have been resolved. There is now a clear consensus that the reaction is assisted by participation of the solvent (water) molecules, which play a critical role in the stabilization of reaction intermediates, regardless of their chemical nature. The insufficient modeling of the solvent environment has thus led to inconsistencies in the theoretical models, resulting in contrasting conclusions.

In the pioneering works on the MEA-CO_2 binding mechanism, Da Silva and Svendsen[105] and Shim *et al.*[106] suggested that the carbamate product is formed *via* a single-step, third-order reaction mechanism. The CO_2 molecule is proposed to bind to one MEA molecule and concurrent deprotonation by a second MEA increases its basicity (Figure 7a). Alternatively, another base or a solvent molecule can substitute the second MEA molecule in the mechanism. In another study, Da Silva and Svendsen recognized a significant stabilization of both the zwitterionic intermediate and the carbamate by the solvent microenvironment and suggested that a zwitterionic intermediate (initially thought to be a transition-state structure) may be present in the (two-step) mechanism (Figure 7b), although it would likely be short-lived.[107]

Arstad *et al.* proposed another mechanism for MEA-CO_2 binding, in which the carbamic acid is formed from the same zwitterionic intermediate through a proton-relay mechanism.[108] In such a pathway, proton transfer is assisted by a solvent (water) molecule or an additional amine species (cf. Figure 7c).

Sumon *et al.* advocated for the use of a more advanced semiexplicit solvation model to obtain accurate energetics, and they included up to 20 water molecules in a hydrogen-bonded cluster around the solutes.[109] A further improved model included the dynamical behavior of the systems obtained from the molecular dynamics. This approach is significantly more demanding, as the advanced evaluation of the free energies along with the sampling of the solvent configurational space is required. As an example of this approach, both mechanisms in Figures 7a,b were re-evaluated by Xie *et al.*[110] Based on *ab initio* calculations (at the CCSD(T) level of theory) combined with quantum mechanics/molecular mechanics/molecular dynamics simulations (QM/MM/MD), the authors concluded that the two-step reaction mechanism to form a carbamate through a zwitterionic intermediate (Figure 7b) is the most likely, contrasting with the "carbamic-acid" pathway. In accordance with the barrier obtained from the experiment, they observed the rate-limiting step to be associated with the MEA(CO_2) formation at ∼50 kJ/mol, which was primarily

https://doi.org/10.1021/acs.chemrev.2c00681
Chem. Rev. 2023, 123, 8069−8098

attributed to the breaking of the hydrogen-bonding network around the CO_2 molecule to initiate binding to MEA.

Employing the (DFT-based) *ab initio* molecular dynamic simulations (AIMD), the stability and mutual interconversion of the reaction intermediates along the two-step CO_2 capture process from Figure 7b (CO_2 + MEA → zwitterion → carbamate) was also studied.[111−117] More specifically, Han *et al.* observed rapid deprotonation of the zwitterionic intermediate, forming a stable carbamate species, which was recognized as the principal driving force for CO_2 absorption.[111] Noticeably, the same zwitterion → carbamate transformation was also supported by the unbiased AIMD, allowing estimation of the zwitterionic intermediate lifetime to be ca. 100 ps.[112]

To some extent, complementary results were later acquired by Guido[112] and by Hwang,[111] which focused on the stability of the zwitterionic intermediate with respect not only to the zwitterion deprotonation (i.e., carbamate formation) but also to CO_2 removal (i.e., MEA regeneration). A delicate balance between the competing pathways was identified in both of the studies, which was deemed to be further complicated by significant temperature and entropic effects that contributed to the free energies from extensive reorganization of the solvent microenvironment. The solvent participation was shown to go far beyond the first solvation shell, providing further evidence of the inadequate use of the continuum (even semiexplicit) solvation models.

The tight balance between zwitterion → carbamate and zwitterion → CO_2 + MEA competition was also acknowledged in investigating CO_2 release from carbamate.[115] Because the calculations revealed that the process is too energetically demanding, the authors made use of the reversibility of the reactions, proposing that CO_2 release is accomplished by (i) regeneration of the zwitterionic intermediate by carbamate protonation by MEA(H^+), and (ii) CO_2 release from the zwitterionic intermediate (i.e., reverse of the reaction pathway B in Figure 7b).

Finally, Matsuzaki *et al.* investigated the mechanism for the formation of the bicarbonate product.[116] Based on the *ab initio* calculations along with the PCM solvation model, they suggested that the formation of the carbamate intermediate (Figure 7b) is followed by its protonation in the next step, yielding the carbamic acid. The carbamic acid is then speculated to further undergo an attack by OH^-, releasing the bicarbonate and free MEA.

Other studies, not directly focused on the mechanism of the CO_2−amine interaction, were carried out to screen the additional effects of molecular structure (e.g., amine substitutions), solvent environment, temperature, and other experimental conditions. A few examples include the calculations of various amine basicities and their correlation with the CO_2 interaction energies (stability of the carbamate intermediate) and/or the reaction kinetics.[105,117−120] Naturally, the electron-withdrawing groups weakened CO_2 binding efficiency as their basicity decreased, and *vice versa*. In addition, Orestes *et al.* proposed that higher basicity implies greater stability of the zwitterionic intermediate, and therefore, suggested that highly basic amines (such as guanidines) may provide relatively stable zwitterions with prolonged lifetimes.[117] This greater stability indicates a stronger bond with CO_2 to form the carbamate through hydrogen atom transfer of the hydrogen atom bound to the amino nitrogen. Jhon *et al.* tried to evaluate steric effects to explain the contrasting patterns in the nucleophilicity of various amines and their reactivity, but further evaluation is needed to predict better CO_2−amine reactivities.[121]

Finally, Li *et al.* evaluated the performance of various exchange-correlation functionals for predicting the MEA−CO_2 interaction.[122] The authors observed somewhat inconsistent results on the optimized geometries and the corresponding energies based on the method that was utilized. In particular, the energetic minima seem to differ significantly when the MP2 or DFT optimizations were performed, which raises concerns as to the accuracy of the *ab initio* single-point calculations carried out on top of the DFT optimized geometries. However, it seems that the ωB97XD functional can be recommended for both optimization and energetic purposes.

In summary, the described theoretical studies have focused on understanding the binding mechanism between amines and CO_2. The primary/secondary amines are believed to react with CO_2 molecules to provide carbamate species through the short-lived zwitterionic intermediate. The strength of the amine−CO_2 interaction is regulated by the basicity (nucleophilicity) of the amines that can, in turn, be controlled by the introduction of the electron-donating/withdrawing substituents. Theoretical studies have also indicated the close participation of the solvent (water) molecules, as these species can stabilize the free reactants (by forming a concise hydrogen-bonding network around them) or particular reaction intermediates (such as zwitterionic intermediate or carbamate) or can function as proton relays to accept/donate protons. Therefore, it comes as no surprise that solvent models that treat water molecules explicitly (or semiexplicitly) exhibit more reliable results than simple continuum-based approaches. On the other hand, the mechanism of CO_2 release is still relatively underexplored, as several contrasting reaction pathways have been suggested.

5. REDOX-ACTIVE CAPTURE MOLECULES

5.1. Introduction

Another popular approach to eCCC is the use of redox-active capture molecules, or redox carriers, that directly bind and release CO_2 upon oxidation or reduction (i.e., direct eCCC methods). Scheme 4 illustrates a generalized direct eCCC cycle featuring a redox carrier.[39] In the cycle, the molecule in the resting state (R) is reduced to form the active state carrier

Scheme 4. Redox-Active Capture Molecules for Electrochemically-Mediated CO_2 Separation, Adapted with permission from ref 39. Copyright 2022 Royal Society of Chemistry.

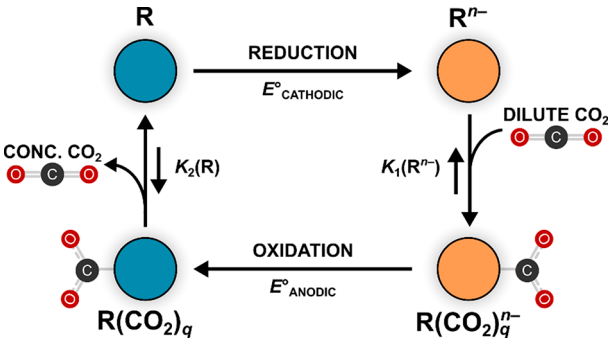

https://doi.org/10.1021/acs.chemrev.2c00681
Chem. Rev. 2023, 123, 8069−8098

Scheme 5. Direct Electrochemical Capture of CO_2 by Quinones via EEC (Black), EECC (Red), or ECEC (Blue) Mechanisms

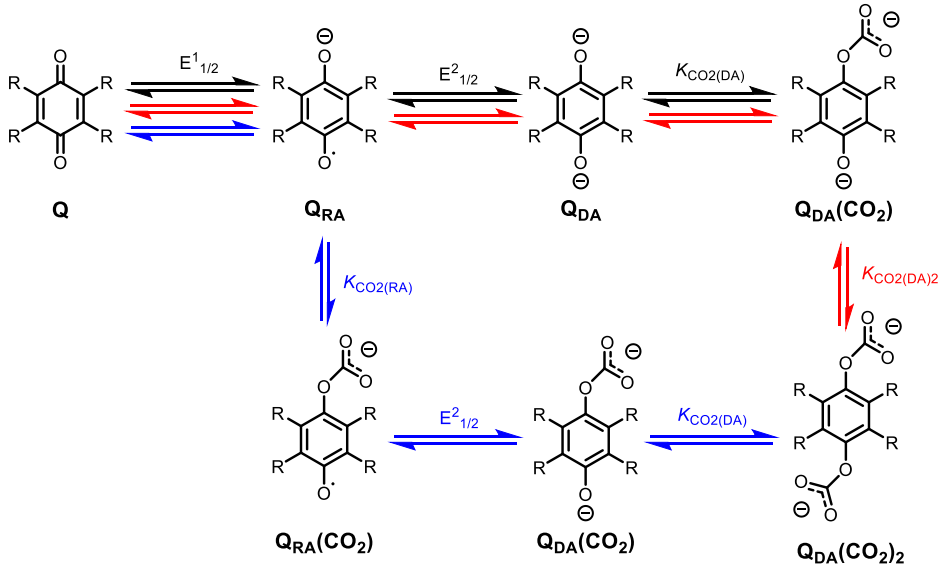

species (R^{n-}), where n is the number of electrons transferred. The reduced species has a high affinity for CO_2 ($K_{1(R^{n-})}$), which allows for capture from a dilute inlet stream to form the CO_2-bound adduct, $R(CO_2)_q^{n-}$. Here, q represents the number of CO_2 molecules that bind to each capture molecule. Release is triggered by the oxidation of $R(CO_2)_q^{n-}$ to form $R(CO_2)_q$, which has a much lower affinity for CO_2 ($K_{2(R)}$), resulting in liberation of CO_2 to reform the resting-state carrier (R) to complete the cycle. This approach takes advantage of the difference between the binding affinity of the oxidized ($K_{2(R)}$) and reduced ($K_{1(R^{n-})}$) states of the carrier (R and R^{n-}, respectively).

DuBois and co-workers were the first to publish the use of redox-active capture molecules for eCCC applications. Several classes of redox-active capture molecules were assessed using spectroscopic, voltammetric, and controlled potential electrolysis approaches to determine both the electrochemical reversibility of CO_2 binding and the CO_2 equilibrium constants of the oxidized and reduced forms.[52,123] In these works, they outline desirable molecular properties of efficient CO_2 capture molecules. They propose that a capture molecule for direct eCCC must have a site capable of CO_2 binding and must also be able to undergo chemically reversible oxidation and reduction in the presence and absence of CO_2. Regarding these two points, they identified the importance of proximity of the redox center to the CO_2 binding site. Shorter distances between the two sites resulted in larger changes in the binding affinity between oxidized and reduced states of the capture molecule. This is important because the difference in CO_2 binding affinity between the oxidized and reduced forms must be sufficiently large to enable sufficient CO_2 capture from a given feed gas. As described in section 2.3, one metric that can be utilized to evaluate if CO_2 is sufficiently captured from the feed gas is the Faradaic efficiency ($\eta_{Faradaic}$), or the moles of CO_2 separated per mole of electron transferred. Assuming complete activation/deactivation of a redox-active capture molecule (with total concentration $[R]_T$), the upper bound on $\eta_{Faradaic}$ for a redox-active carrier/solvent system can be determined using eq 9. This expression was derived using equations presented by Clarke *et al.*, and aligns with other previous works.[123−125] More information on the derivation of eq 9 is presented in the Notes section at the end of the review.

$$\eta_{Faradaic} = \frac{q}{n}\left(\frac{K_{1(R^{n-})}(K_H P_i)^q}{1 + K_{1(R^{n-})}(K_H P_i)^q} - \frac{K_{2(R)}(K_H P_f)^q}{1 + K_{2(R)}(K_H P_f)^q}\right) - \frac{K_H}{n[R]_T}(P_f - P_i) \quad (9)$$

In the above equation, K_H is the Henry's law constant for CO_2 in the electrolyte (M atm^{-1}), P_i is the initial CO_2 partial pressure before separation (atm), and P_f is the final CO_2 partial pressure after separation and recovery (typically 1 atm). For any capture molecule, the upper bound on achievable Faradaic efficiencies is q/n. Then, considering an example system with a 10% CO_2 feed gas (within the typical concentration range for a coal-fired power plant flue gas)[19,24] and the following constant parameters ($[R]_T$ = 1 M, K_H = 0.175 M atm^{-1}, $K_{2(R)} \ll 1$, n = 2, and q = 1), a $K_{1(R^{n-})}$ value of at least 6.3×10^2 is required to obtain ≥90% of the maximum Faradaic efficiency (q/n) according to eq 9. Using the same equation, a $K_{1(R^{n-})}$ value of at least 1.6×10^5 is necessary to capture from atmospheric CO_2 sources (P_i = 410 ppm) with the same efficiency.

In addition to impacting the Faradaic efficiency, binding coefficients can also influence system energy requirements due to their direct relation to the difference in standard potentials for the binding and release steps ($\Delta E = E^\circ_{cathodic} - E^\circ_{anodic}$). More specifically, ΔE is logarithmically proportional to the ratio between the activated and deactivated capture molecule binding affinities, i.e., $K_{1(R^{n-})}/K_{2(R)}$, according to eq 10.

$$\Delta E = -\frac{RT}{nF}\ln\left(\frac{K_{1(R^{n-})}}{K_{2(R)}}\right) \quad (10)$$

Therefore, a higher binding affinity ratio, $K_{1(R^{n-})}/K_{2(R)}$, may lead to higher cell voltages and thus greater energy requirements. To further assess this trade-off between system energy requirements and Faradaic efficiency, Clarke *et al.* defined a combined efficiency metric to highlight molecular properties (such as $K_{1(R^{n-})}$) that may adequately balance this trade-off.[125] Their work also explores how these effective properties are

https://doi.org/10.1021/acs.chemrev.2c00681
Chem. Rev. 2023, 123, 8069−8098

Table 1. Reported Reduction Potentials for Various Quinone Radical Anion/Dianion Redox Pairs ($E^2_{1/2}$) and Associated CO_2 Binding Constants of the Dianion Species ($K_{CO2(DA)}$)

quinone	solvent	$E^2_{1/2(N2)}$ [a]	$E^2_{1/2(CO2)}$ [a]	$\Delta E_{1/2}$ [b]	log($K_{CO2(DA)}$)	ref
tetrafluoro-1,4-benzoquinone	DMF	−0.80	−0.50	0.30	4.3	135
tetrabromo-1,4-benzoquinone	DMF	−0.88	N/A	N/A	3.3	139
2,3-dichloro-1,4-naphthoquinone	DMF	−1.21	N/A	N/A	5.7	139
2,5-bis(dimethylamino)-3,6-difluoro-1,4-benzoquinone	DMF	−1.47	N/A	N/A	11.6	139
tetrachloro-1,4-benzoquinone	MeCN	−0.72	N/A	N/A	3.8	52
2,6-di-*tert*-butyl-1,4-benzoquinone	MeCN	−1.46	N/A	N/A	15.0	52
9,10-phenanthrenequinone	MeCN	−1.19	N/A	N/A	11.8	52
2,3-dicyano-1,4-benzoquinone[c]	MeCN	−0.47	N/A	N/A	3.8	123
2,6-dichloro-1,4-benzoquinone	MeCN	−0.94	−0.60	0.34	6.0	127
2-chloro-1,4-benzoquinone	MeCN	−1.07	−0.58	0.49	10.0	127
tetrafluoro-1,4-benzoquinone	MeCN	−0.80	−0.62	0.18	3.8	127
tetrachloro-1,4-benzoquinone	MeCN	−0.74	−0.63	0.11	2.5	127
5-hydroxy-NQ[d]	MeCN	−0.94	−0.71	0.23	3.3	127
1,8-dihydroxy- AQ[d]	MeCN	−1.20	−0.94	0.26	5.4	127
1,2-dihydroxy- AQ[d]	MeCN	−1.29	−1.08	0.21	4.6	127
5,8-dihydroxy- NQ[d]	MeCN	−0.98	−0.91	0.07	2.1	127
anthraquinone	MeCN	−1.56	−0.62	0.46	9.0	140
1-hydroxy-AQ[d]	MeCN	−1.30	−1.18	0.20	5.1	140
1,4-dihydroxy-AQ[d]	MeCN	−1.15	−1.14	0.01	1.1	140
1-amino-AQ[d]	MeCN	−1.58	N/A	N/A	8.3	140
1,4-diamino-AQ[d]	MeCN	−1.63	N/A	N/A	9.7	140
1-amino-4-hydroxy-AQ[d]	MeCN	−1.41	−1.20	0.21	4.8	140
2,3-dicyano-1,4-naphthoquinone	MeCN	−0.62	N/A	N/A	1.7	139
2,5-bis(dimethylamino)-1,4-benozquinone	MeCN	−1.23	N/A	N/A	12.1	139
tetra(dimethylamino)-1,4-benzoquinone	MeCN	−1.68	N/A	N/A	11.6	139
tetramethylester-1,4-benzoquinone	$CHCl_3$	−0.65	N/A	N/A	2.5	139

[a]Potentials are reported as V vs SCE. Potentials recorded in MeCN were converted to SCE using ref 141. [b]Reported in units of volts and equal to the shift in half-wave potential in the presence and absence of CO_2 ($\Delta E_{1/2} = E^{o\prime} - E_{1/2}$ in eq 11). [c]Undergoes Kolbe−Schmidt reaction with CO_2 as a decomposition pathway. [d]Features intramolecular hydrogen-bonding interactions. Calculated using eq 11 from reported reduction potentials under N_2 and CO_2 atmosphere.

dependent upon other system properties such as system configuration.

Beyond having adequate CO_2 binding affinities while maintaining a minimal potential difference between binding and release steps, additional desirable characteristics of capture molecules include rapid electron transfer kinetics, high solubility, stability of the carrier species toward other compounds present in a given feed gas composition (e.g., oxygen, water vapor), among others.[38,39,124] Overall, several different classes of molecules have been identified and assessed as capture molecule candidates. Quinones are the most studied group of molecules,[112,115,124,126−129] but other redox-active capture species have been assessed as well, including transition-metal complexes,[130] bipyridines,[131−133] and thiols.[134] In the following sections, several demonstrations involving different capture molecules and solvents will be discussed. These demonstrations include primarily cyclic voltammetry and bulk electrolysis experiments to assess CO_2 binding/release capabilities, as well as a few engineered flow-cell systems.

5.2. Mechanistic Insights and Demonstrations

5.2.1. Quinones. Quinones can also bind CO_2 directly under aprotic conditions. CO_2 reacts with reduced quinones at one or more anionic oxygen atoms *via* an ECEC (electron transfer, chemical reaction, electron transfer, chemical reaction), EECC (two electron transfers followed by two chemical reactions), or EEC (electron transfer, electron transfer, chemical reaction) mechanism.[127] An ECEC mechanism may be desirable because the quinone captures two CO_2 molecules, increasing the sorbent capacity. Additionally, capturing two CO_2 molecules per two electron transfers theoretically allows for Faradaic efficiencies of 100%. ECEC or EEC mechanisms depend on whether CO_2 molecules bind to the reduced species in its radical anion (Q_{RA}) and/or dianion (Q_{DA}) forms (Scheme 5).[126−128] In general, quinones have displayed a wide range of affinity for CO_2; reported CO_2 binding constants for quinone dianions ($K_{CO_2(DA)}$) have been between ca. 10 and 10^{20}, which is summarized in Table 1. Numerous quinones also bind CO_2 in their radical anion state (Q_{RA}). However, to date, $K_{CO_2(RA)}$ values have only been reported for 9,10-phenanthrenequinone and 2,6-di-*tert*-butyl-1,4-benzoquinone.[52,123] The binding constants for both radical anions ($K_{CO_2(RA)}$) were several orders of magnitude smaller than the corresponding values for the dianions ($K_{CO_2(DA)}$). Although no other values of $K_{CO_2(RA)}$ have been quantitatively determined, cyclic voltammetry suggests that $K_{CO_2(RA)}$ is always much smaller than $K_{CO_2(DA)}$,[52,123,127,128,135,136] likely due to increased nucleophilicity of the oxygen atoms in the dianion. The specific value for $K_{CO_2(RA)}$, which represents the thermodynamic favorability of CO_2 binding to a quinone radical anion species, causes the disparity in reported mechanisms (EEC or ECEC). A complication to this assessment, however, is if disproportionation of two Q_{RA} molecules transpires to create Q and Q_{DA}, which then reacts with CO_2; this may result in inflated values for $K_{CO_2(RA)}$ and

https://doi.org/10.1021/acs.chemrev.2c00681
Chem. Rev. 2023, 123, 8069−8098

falsely suggest an ECEC mechanism if not properly considered.[123,137,138]

Among the multiple classes of redox-active molecules first considered by DuBois and co-workers, quinones were the most promising because they have a CO_2 binding site, are able to undergo a reversible reduction and oxidation in both the presence and absence of CO_2, and have a significant CO_2 binding affinity in the activated form and little to no binding affinity in the deactivated form.[52] A wide variety of quinone candidates were screened in acetonitrile (MeCN) and dimethylformamide (DMF) using both cyclic voltammetry and bulk electrolysis techniques. Of the large number investigated, only five showed reversible CO_2 binding and release with sufficient CO_2 binding affinities: 2,6-di-*tert*-butyl-1,4-benzoquinone (DtBBQ), 9,10-phenanthrenequinone (PAQ), tetrachloro-1,4-benzoquinone (TCQ), 2,3-dicyano-1,4-benzoquinone, and 2,3-dicyano-5,6-dichloro-1,4-benzoquinone (DDQ). Reduction potentials and values of $K_{CO_2(DA)}$ (and some values of $K_{CO_2(RA)}$) were reported for each of the five quinones, however, little mechanistic information was determined beyond the number of CO_2 molecules bound per quinone dianion. A significant observation in this work was that the CO_2 binding affinities of the quinone dianions ($K_{CO_2(DA)}$) were linearly correlated with the reduction potentials. This trend has since been observed among a wider selection of quinones,[39,123,127,142−144] bipyridines,[142] and more recently with N-heterocyclic carbene (NHC) analogues (using DFT-derived binding constants).[145]

In 1989, Mizen and Wrighton reported the first mechanistic study of CO_2 binding to quinone dianions.[126] Chemical reduction of PAQ was used to characterize the CO_2-active species. PAQ was reduced by one or two electrons with cobaltocene or sodium metal (to form $PAQ^{\bullet-}$ or PAQ^{2-}, respectively), followed by addition of CO_2 resulted in the formation of a new species. This species featured a ^{13}C NMR peak between 156 and 158 ppm in CD_3CN or DMSO-d_6, suggesting formation of an alkyl carbonate. Infrared spectroscopy further confirmed this assessment, exhibiting carbonyl stretches at 1646 and 1686 cm^{-1} when cobaltocene was used as the reductant. Spectroelectrochemical infrared (SEC-IR) spectroscopy indicates the formation of a single carbonyl stretch at 1646 cm^{-1} upon reduction of PAQ to PAQ^{2-}. The stretch observed at 1686 cm^{-1} was attributed to interactions with the cobaltocenium cation, which is more likely to interact and stabilize the CO_2 adduct than the tetrabutylammonium cations present in SEC-IR studies. When the same experiments were repeated in the absence of CO_2, the ^{13}C NMR and IR signals were not observed, which indicated CO_2 binding occurs at one or both anionic oxygen atoms upon reduction of PAQ to PAQ^{2-}. With this information, along with the experimentally determined 2:1 ratio of CO_2:PAQ^{2-}, Mizen and Wrighton proposed an ECEC mechanism for the reaction whereby two molecules of CO_2 are bound through the two oxygen atoms of PAQ^{2-}.

Shortly thereafter, Ogura and co-workers reported a mechanistic study with several other quinones and CO_2 in MeCN.[127] This study expanded upon the work of Mizen and Wrighton by including 11 different quinones of varying electron density. Like PAQ, the quinones with more nucleophilic oxygen atoms were found to bind two molecules of CO_2 *via* an ECEC mechanism. In contrast, the less electron dense quinones did not bind CO_2 in the radical anionic state and thus were proposed to undergo an EEC to bind one molecule of CO_2 upon reduction to the dianion. Interestingly, the authors observed that there appeared to be a specific threshold potential for the first reduction (to form the radical anion) where the quinones switched between EEC and ECEC mechanisms. The proposed ECEC mechanism for 1,4-anthraquinone (AQ), 1,4-naphthoquinone (NQ), duroquinone (DQ), and 2,6-dimethylbenzoquinone (DMQ) in MeCN by Ogura and co-workers contrasts with the mechanism previously reported in dimethylsulfoxide by Simpson and Durand.[136] Simpson and Durand proposed an ECE mechanism for each of these quinones based on cyclic voltammetry; however, the authors did not determine how many CO_2 molecules were bound to the reduced quinone species. Due to the difficulty of differentiating ECE and ECEC mechanisms by cyclic voltammetry and without knowledge of neither reaction stoichiometry nor products formed,[146] it is likely that the mechanism was incorrectly assigned and is in fact ECEC for these quinones. In more recent work, naphthoquinones have been determined to undergo ECEC or EEC mechanisms in ionic liquid solvents, similar to what has been previously observed in aprotic organic solvents.[128]

To study the redox behavior and the reactivity toward CO_2 capture of *p*-benzoquinone (BQ) and tetrafluoro-*p*-benzoquinone (TFBQ), Namazian *et al.* employed both experiments (cyclic voltammetry) and theory (*ab initio* calculations with the G3MP2//B3LYP composite method with the CPCM solvation model).[135] Their cyclic voltammetry results in a DMF solvent indicated that BQ is likely to capture CO_2 after the first reduction to the BQ semiquinone ($BQ^{\bullet-}$), whereas TFBQ was proposed to react with CO_2 only after the two-electron reduction ($TFBQ^{2-}$) is accomplished (note that this corresponds to the ECE and EEC mechanisms for BQ and TFBQ, respectively). In the article, the lower reactivity of the TFBQ semiquinone was explained based on the lower nucleophilicity of the quinone's oxygen atoms due to the presence of the electron-withdrawing fluorine atoms. The calculation of the lower charge on the oxygen atoms in $TFBQ^{\bullet-}$ was performed as a confirmation. The BQ and TFBQ molecules were also compared in terms of the regioselectivity of CO_2 binding. Both theory and experimental work indicate that $TFBQ^{2-}$ binds CO_2 at the oxygen atom, forming a carbonate product (note that the carbonate was calculated to be favored by ∼88 kJ/mol over the carboxylate). Comparatively, theory predicts that BQ^{2-} prefers carboxylate (carbon-bound CO_2) over the carbonate product by ∼10 kJ/mol.[138] However, these findings conflict with previous experimental observations, and they speculated that this difference may be due to kinetics, as the formation of the carbonate product may be a faster reaction than that to form the more stable carboxylate product. While formation of a carboxylate versus a carbonate does not affect the overall mechanism (i.e., EEC or ECE) in theory, it is unclear if and how the resulting product would impact overall performance of a redox-active capture molecule. Fan *et al.* revisited the BQ reactivity by comparing the properties of the most stable carboxylate species obtained from the calculations with the experimental infrared absorption, and notably, the authors' findings were in agreement.[147]

Naphthoquinones undergo ECEC or EEC mechanisms in ionic liquid solvents, similar to what has been observed in aprotic organic solvents.[128] Jin and co-workers used a spectroelectrochemical approach to elucidate the mechanism

https://doi.org/10.1021/acs.chemrev.2c00681
Chem. Rev. 2023, 123, 8069−8098

and site of binding for CO_2 capture with NQ, 2-chloro-1,4-napthoquinone (CNQ), and 2,3-dichloro-1,4-napthoquinone (DCNQ). Upon two electron reductions of NQ to the dianion (NQ^{2-}) under CO_2, a carbonyl stretch is observed at 1634 cm^{-1} *via* spectroelectrochemical infrared spectroscopy (SEC-IR). The IR band is consistent with a carbonate species and is not present when the experiment is repeated in an inert N_2 atmosphere. This result suggests that CO_2 binds to NQ^{2-} through the anionic oxygen atoms, similar to what was previously observed with PAQ^{2-} in MeCN.[126] Using cyclic voltabsorptometry (CVA) and derivative cyclic voltabsorptometry (DCVA), the authors concluded that the reaction of CO_2 with NQ follows an ECEC mechanism. By monitoring the IR spectrum during CVA and DCVA experiments, it was observed that the CO_2 binds to the radical anion ($NQ^{\bullet-}$) prior to being reduced to the dianion, where it could then bind a second molecule of CO_2. The overall reaction stoichiometry of NQ with CO_2 was further confirmed by Ogura and co-workers using a similar method.[127] When the solution was oxidized, the carbonate stretch at 1634 cm^{-1} disappeared, with the growth of a peak at 1671 cm^{-1} corresponding to NQ. This pattern was observed across multiple consecutive scans, indicating that binding and release is reversible. When these experiments were repeated for CNQ and DCNQ, similar results were observed; however, both quinones only bind one molecule of CO_2 through a proposed EEC mechanism.

In a recent study, Alherz and co-workers proposed that CO_2 binding to reduced quinones occurs exclusively *via* EEC or EECC mechanisms.[144] Seven different quinones were investigated, and DFT was used to estimate the number of CO_2 molecules bound to each dianion at varying $[CO_2]$. The binding stoichiometry at higher concentrations ($[CO_2] \geq 5\%$) was supported experimentally *via* cyclic voltammetry. The less reducing quinones (tetrachloro-1,4-benzoquinone and 2,3-dichloro-1,4-napthoquinone) were reported to bind one CO_2 molecule at $[CO_2] \geq 5\%$ *via* an EEC mechanism, while the other four capable of CO_2 binding (2,6-dichloro-1,4-benzoquinone, 1,4-benzoquinine, 2,6-dimethyl-1,4-benzoquinone, and 1,4-napthoquinone) bind two CO_2 molecules *via* an EECC mechanism. The authors argue that the latter quinones undergo an EECC rather than ECEC mechanism as there is no significant anodic shift in the first reduction potential (to the quinone radical species) observed in the presence of CO_2. While this mechanism should always be considered as a possibility when investigating new quinone eCCC carrier candidates, other spectroscopic studies indicate an ECEC mechanism for 1,4-napthoquinone[128] and 1,4-benzoquinone[147] (in addition to the studies on other quinones discussed in the current section of this review). While thermodynamic data exist for CO_2 binding with various quinone dianion species and some anion species, much less kinetic information has been reported. Yet, CO_2 reaction kinetics will play an important role in overall system performance as they will influence the rate of CO_2 binding/release and, consequently, the design and performance of associated process units (e.g., absorption column). In early work, Wrighton and DuBois investigated the kinetics of binding between quinones (PAQ and DtBBQ, respectively) and CO_2 following reduction. Using chronoamperometric techniques, they obtained second-order rate constants of 96 and 19.1 M^{-1} s^{-1} for $PAQ^{\bullet-}$ in MeCN and $DtBBQ^{\bullet-}$ in DMF, respectively.[123,126] Durand and co-workers performed a kinetic investigation of CO_2 binding with a series of quinones in DMSO.[136] Using rotating disk voltammetric methods, the second-order rate constants for five quinones were determined, ranging between 46 to 350 M^{-1} s^{-1}. The second-order rate constants were derived using digital simulations based on data obtained under pseudo-first-order conditions, instead of through varying the concentrations of CO_2 as was done in prior studies. Results from the five quinones indicate that there may be a relationship between the first (more oxidative) reduction potential and CO_2 binding rate constant, such that more negative reduction potentials (more nucleophilic quinones) correspond with faster binding. However, relatively large errors in the rate constants and the small data set prevents analysis of any observed trends. While it is currently unclear what rate constant values will be required or optimal, there are indications for how rate constants could impact CO_2 binding selectivity. From the limited data reported for quinone-CO_2 reactivity, protonation is confirmed to be kinetically favored.[136,138] For example, protonation of anthraquinone has been observed to be twice as fast as CO_2 binding in DMSO.[136] If an electrochemical separation process requires CO_2 removal from a mixture with high water vapor concentrations, relatively slow CO_2 binding kinetics (as compared to protonation) could significantly reduce capture molecule effectiveness. Thus, careful matching of solvent and quinone pK_a values and/or preclusion of acidic proton sources are necessary to prevent kinetic inhibition of eCCC due to protonation.

In addition to these mechanistic studies, quinones have also been cycled over longer time scales using controlled potential electrolysis or other electrochemical techniques to quantitatively demonstrate CO_2 capture and release. Scovazzo *et al.* reported a successful proof-of-concept CO_2 capture and release system for direct eCCC, which used solutions of DtBBQ in either propylene carbonate or 1-butyl-3-methylimidazolium hexafluorophosphate ionic liquid ($[bmim][PF_6]$).[124] Using a closed-system bulk electrolysis setup, the authors demonstrated that direct eCCC from very dilute (<1%) inlet streams was plausible and that the overall CO_2 concentration could be increased to near 100% upon oxidation in a single pass. Using 30 mL of the propylene carbonate solution (0.30 M DtBBQ and 0.75 M tetrabutylammonium tetrafluoroborate supporting electrolyte), 120 mL of pure CO_2 was captured and then released from an incoming 0.5% CO_2 inlet stream. Successful capture, release, and concentration was also performed using $[bmim][PF_6]$ as the solvent and electrolyte. However, the low concentration of DtBBQ compared to the solubility of CO_2 in $[bmim][PF_6]$ (0.05 M versus 0.08 M/atm, respectively) resulted in a less impressive concentration swing, which ranged between 7% to 33% initial and final concentrations. In the two demonstrations, 0.427 and 0.454 mol of CO_2 were released per mole of electron in PC and $[bmim][PF_6]$, respectively, resulting in Faradaic efficiencies of ∼43% and ∼45%. These Faradaic efficiencies compare well to the maximum Faradaic efficiency of 50% for DtBBQ, as it requires two electron-transfer steps for binding and release, but only one molecule of CO_2 is bound to the dianion. The estimated energetic efficiency of the system is unclear, as no electrode potential difference between the capture and release steps was reported. However, typical bulk electrolysis cells (often referred to as "H-cells"), as such, are nonoptimized for high performance operation, and thus, any reported energetic efficiency would likely not be representative of this system's potential.

https://doi.org/10.1021/acs.chemrev.2c00681
Chem. Rev. 2023, 123, 8069−8098

Hatton and co-workers developed a more engineered cell architecture by using polymeric quinone-based electrodes for eCCC processes (Figure 8).[148] Their approach, coined

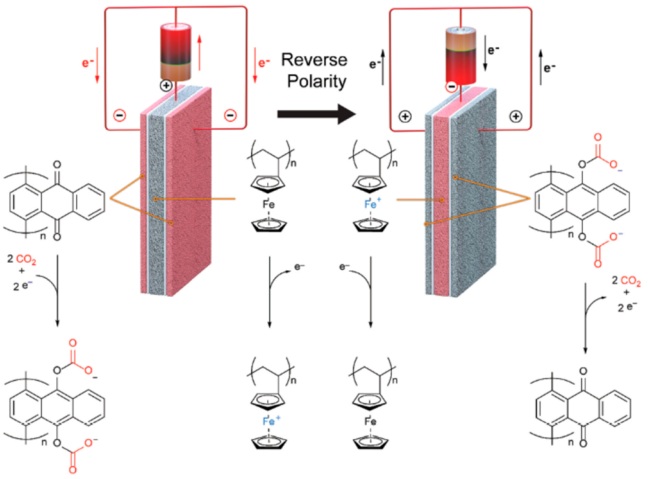

Figure 8. Faradaic electro-swing system with a polymeric anthraquinone electrodes for direct eCCC developed by Voskian and Hatton. Reproduced from ref 144 under the CC BY 3.0 license.

"electro-swing reactive adsorption" (ESA), uses a carbon fiber cathode coated in a suspension of carbon nanotubes (CNTs) and a polymeric anthraquinone (p-AQ) that adsorbs CO_2 directly to the electrode surface upon reduction. To complete the cell, a carbon fiber anode coated in CNT and polyvinyl ferrocene was used. In their first demonstration, the ionic liquid 1-butyl-3-methylimidazolium bis(trifluorosulfonyl) imide ([bmim][Tf_2N]) served as both the solvent and supporting electrolyte. The Faradaic efficiency of the system was 90% based on cycling experiments performed in a sealed container under a 100% CO_2 atmosphere. In this demonstration, the cell potential was controlled and switched between −1.3 and 0.5 V, while the headspace pressure was monitored to track CO_2 uptake and release by the p-AQ electrode. In addition to sealed cell measurements, an open cell setup was used where a dilute CO_2 stream was passed through an adsorption bed composed of multiple cells. In this setup, the p-AQ electrodes performed quantitative capture from 10% CO_2 inlet streams, where over 80% capture was observed with inlet stream concentrations as low as 0.6%. Additionally, the system was quite robust, with ∼30% degradation after 7000 capture/release cycles. Based on the applied potential difference and Faradaic efficiency (90%), the reported system energy requirements were 90 kJ/mol CO_2 for CO_2 removal and recovery from a 10% CO_2 concentration (with N_2 balance). Based on the reported values, the experimental energetic efficiency of the system is estimated to be ca. 6% (given that a 10% to 100% swing for a case of "skimming" requires 5.7 kJ/mol CO_2). The authors also hypothesize that after several cycles, ΔE can be dropped to 500 mV where ∼60% of the quinone species are activated for capture. Although it was never evaluated experimentally, dropping ΔE to 500 mV is estimated to lower the energetic requirement to ∼43 kJ/mol CO_2 (which increases the energy efficiency to ∼13%).

More recently, Hatton and co-workers have used their p-AQ electrodes with "water-in-salt" electrolyte mixtures in place of ionic liquids.[149] Large concentrations of lithium bis-(trifluoromethylsufonyl)imide (LiTFSI) in water results in a significant extension of the electrochemical window, such that p-AQ could be reduced and oxidized while minimizing solvent or electrolyte side reactions. Due to the reduced concentration of "free-state" water present in 20 m LiTFSI at pH 4 (where m is molality), protonation of the reduced p-AQ species was suppressed. Due to high supporting salt concentrations, this reactivity runs counter to what has been observed with other quinones in aqueous media[77,78] as well as what was observed with p-AQ electrodes in 1 m NH_4NO_3 at the same pH. Limited proton availability also results in a more anodic potential for the oxygen reduction reaction, decreasing the sensitivity of p-AQ to O_2. Additionally, unlike other reported examples of quinones in the presence of alkali metals,[150−155] the reduction potential of p-AQ does not shift anodically with increasing concentration of LiTFSI (from 1 to 20 m) under an inert N_2 atmosphere. When CO_2 was introduced, the reduction peak did shift anodically, indicating the formation of the CO_2 adduct, quinone bis(carbonate). The adduct was also observed to be oxidized at more positive potentials than the p-AQ dianion. Increasing concentrations of LiTFSI under CO_2 resulted in increased separation between the reduction and oxidation potentials, which was attributed to stabilization of p-AQ CO_2 adducts by LiTFSI, as confirmed by DFT.[148] Using their electro-swing operation strategy with a custom "zero-gap" flow cell, CO_2 binding and release cycles were performed at currents of up to 2 mA cm^{-2} (2 A g^{-1}). While operating under constant current conditions of 0.5 mA cm^{-2}, the authors reported an energetic requirement of ∼56 kJ/mol CO_2 for their system in 20 m LiTFSI, an improvement over the demonstration in [bmim][PF_6], as described above. Based on the reported energy requirement for capture from an initial CO_2 concentration of 15%, an estimated overall efficiency of at least 8% is calculated (given that a 15−100% swing requires a minimum of 4.7 kJ/mol CO_2 for the case of "skimming"). The system displayed the same excellent stability that was previously observed in [bmim][PF_6], while also operating in the presence of oxygen. A Faradaic efficiency of over 95% was averaged over 75 cycles in 20 m LiTFSI under a gas composition of 15:3:82 CO_2:O_2:N_2. Hatton and co-workers continued to add alkali metals, albeit at lower concentrations (1 M NaTFSI), in their work with 2,3-di-(2-(2-methoxyethoxy)ethoxy)-1,4-naphthoquinone, which is a liquid quinone.[156] Here, they demonstrated capture from a 15% CO_2 mixture (85% N_2), operating at ca. 70% Faradaic efficiency (analagous to their CO_2 capacity utilization efficiency metric) while maintaining relatively low levels of efficiency decay over 10 cycles. When 5% O_2 was added to the mixture, efficiency losses were increased, and thus the authors emphasized that understanding O_2 reduction rates in this system will be a focus of future work. They also developed a continuous flow lab-scale test system and demonstrated CO_2 capture and release from a pure CO_2 stream (due to limitations on quinone conversion) and estimated that cell energy requirements could be in the range of 35−220 kJ/mol CO_2.

Recently, to address the observed instability of quinone carriers in the presence of O_2, Zito *et al.* investigated the validity of the previously observed linear relationship between the second reduction potential and CO_2 binding constant of quinones.[139] In their work, they synthesized and tested the ability of seven new quinones to capture CO_2 in their dianion states. The measured $K_{CO_2(DA)}$ values were in the range of ca.

https://doi.org/10.1021/acs.chemrev.2c00681
Chem. Rev. 2023, 123, 8069−8098

50−10^{12} and followed the trend of decreasing reduction potentials with increasing $K_{CO_2(DA)}$. The experimental investigation was complemented by large-scale DFT calculations oriented on understanding how the substituent effects on the quinone scaffold influence the key thermodynamic properties (such as reduction potentials and CO_2 binding constants) through steric and electronic effects. Overall, Zito *et al.* found that the linear trend holds relatively well over a large range of reduction potentials, suggesting that additional secondary interactions might be required to shift the reduction potentials more positive than the O_2 reduction reaction. This could be achieved, e.g., *via* auxiliary binding charged groups or hydrogen bond donors.

The effects of hydrogen bond donors was probed by Barlow *et al.*, who demonstrated that the use of such additives indeed shifts the reduction potential of the redox-active capture molecule to more positive potentials.[142] Different alcohols were added to tetrachloroquinone (TCQ) in DMF to study the effect of these hydrogen-bond donors on the reduction potential and the CO_2 binding affinity. Although all alcohol additives resulted in a positive shift of the reduction potential, stronger hydrogen-bonding interactions inhibited CO_2 binding, leading to smaller CO_2 binding affinities, while moderate interactions resulted in larger CO_2 binding affinities. Ethanol was identified as a hydrogen-bond donor that did not have deleterious effects on the CO_2 binding affinity but enabled a favorable shift in the reduction potential to values greater than that of O_2 reduction. TCQ was tested *via* controlled potential electrolysis with the presence and absence of ethanol in the electrolyte mixture, where the reduced form of TCQ (TCQ^{2-}) was oxidized and rereduced in the presence of a simulated flue gas mixture (87:10:3 N_2:CO_2:O_2). With ethanol as an additive, Barlow *et al.* showed improvements in the extent of electrochemical CO_2 capture and concentration from flue gas concentrations in the presence of O_2. More specifically, with the addition of ethanol, the estimated Faradaic efficiencies during both oxidation/release and reduction/recapture steps were improved from 84% to 95% and 27% to 73%, respectively. The TCQ/ethanol pair was not tested over multiple cycles, so long-term stability of this specific chemistry is unclear. However, this work demonstrates that hydrogen-bond donors can be added to an electrolyte to anodically shift the reduction potentials of the quinone (or another redox-active capture agent) and improve O_2 stability.

5.2.2. Transition Metals. Redox-active transition metal (TM) centers paired with specific ligands can also serve as CO_2 capture agents in direct eCCC systems. DuBois and co-workers suggested that TM complexes with ligands that contain a CO_2 binding site (i.e., a nucleophilic nitrogen or oxygen) could enable CO_2 pumping.[123] The metal center as the active redox site would alter the electron density of the compound and thus the CO_2 binding affinity. Their study found that the distance between the redox metal center to the CO_2 binding site significantly impacts the compound's ability to capture and release CO_2. The assayed compounds contained one, two, or five atoms separating the binding site to the redox active metal center of Co, Fe, or Ru. CO_2 capture activity was only observed in the Co^{3+} cyclopentadienyl indenyl complex with a one-atom separation of the metal from the binding site.

A few binuclear TM complexes explored in other works were demonstrated to trap CO_2 dissolved in aqueous media as a bound carbonate ion.[157−160] In these complexes, specific bridging ligands orient two metals (Zn, Co, Ni, or Cu) to issue strong carbonate binding interactions. However, studies examining the electrochemical behavior of these compounds and their application to reversibly pumping CO_2 are limited.

DuBois and co-workers examined binuclear Ni and Cu complexes with varied bridging ligands for the reversible capture and release of bicarbonate and found that more flexible ligands resulted in enhanced binding.[130,160] However, the reduction potentials of the nickel complexes were too negative for electrochemical pumping. Of the copper complexes surveyed, the $[Cu_2(tpmc)(\mu\text{-}OH)]^{3+}$ complex (tpmc = bridging *N*,*N*′,*N*″,*N*‴-tetrakis(2-pyridylmethyl)-1,4,8,11-tetraazacyclotetradecane ligand), demonstrated a viable reduction potential for CO_2 pumping and successful electrochemical CO_2 capture and concentration from 10% to 75% (Figure 9).

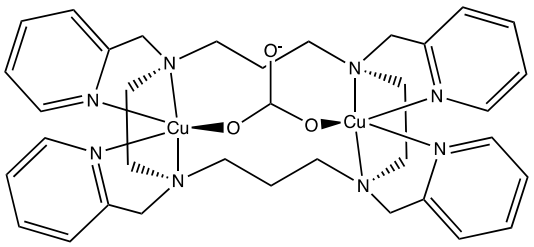

Figure 9. Carbonate adduct, $[Cu_2(tpmc)(\mu\text{-}CO_3)]^{2+}$ formed from $[Cu_2(tpmc)(\mu\text{-}OH)]^{3+}$.

Cycling resulted in partial precipitation of the Cu^+ complex, an outcome which could potentially be improved upon with variation of supporting electrolytes or ligand. DuBois and co-workers examined binuclear Ni and Cu complexes with varied bridging ligands for the reversible capture and release of bicarbonate. Contrary to typical increased CO_2 binding affinity upon reduction, these systems bind carbonate upon *oxidation* and *reduction* results in CO_2 release. In their work, they found that more flexible ligands resulted in enhanced binding.

5.2.3. Pyridines and Bipyridines. Bipyridines also become more nucleophilic upon reduction, making them suitable candidates as CO_2 capture redox carriers. A study by Ishida *et al.* described the reversible capture and release of CO_2 by *N*-propyl-4,4′-bipyridinium ($Prbipy^+$).[131] More recently, Buttry and co-workers explored the reactivity of the related *N*-methyl-4,4′-bipyridinium ($Mebipy^+$) with experimental data and theoretical calculations.[132] The electrochemical behavior and DFT calculations indicate that $Mebipy^+$ (and the related $Prbipy^+$) follow the CO_2 binding mechanism shown in Scheme 6. First, the $Mebipy^+$ is reduced by one electron to form a neutral $Mebipy^\bullet$. In the presence of CO_2, $Mebipy^\bullet$ species

Scheme 6. Reduction of $MeBipy^+$, Disproportionation of $Mebipy^\bullet$, and CO_2 Binding to $Mebipy^-$

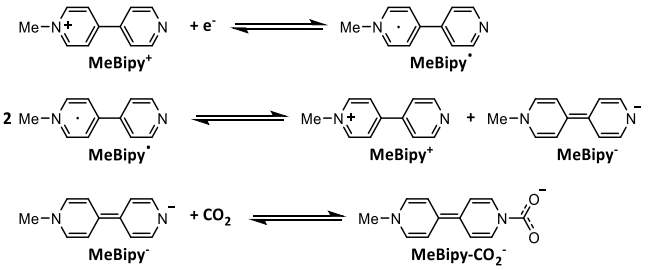

https://doi.org/10.1021/acs.chemrev.2c00681
Chem. Rev. 2023, 123, 8069−8098

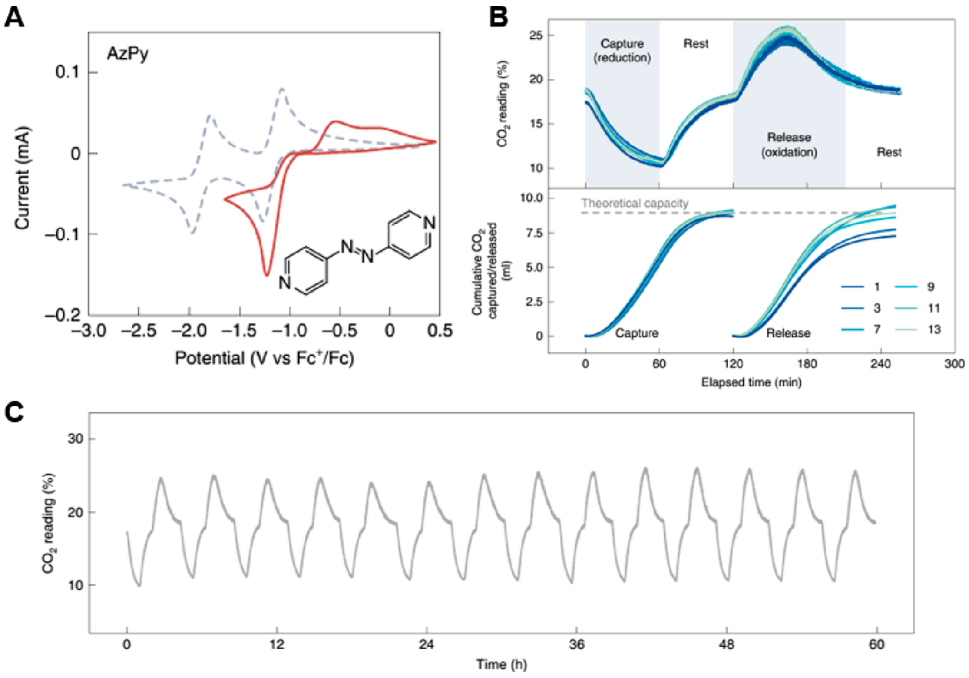

Figure 10. (A) Cyclic voltammograms of 4,4′-azopyridine under N_2 (dashed line) or CO_2 (solid line) atmosphere in DMSO using 0.1 M tetrabutylammonium hexafluorophosphate as a supporting electrolyte. (B) (top) CO_2 readings for selected capture−release cycles. (bottom) Cumulative amounts of CO_2 captured and released in each cycle relative to theoretical capacity. (C) Headspace CO_2 readings over 14 repeated capture and release cycles. The experimental setup to obtain the experimental data shown in parts B and C involved continuous sparging of the azopyridine-containing tank (containing 0.2 M azopyridine capture agent in DMSO with 0.5 M NaTFSI supporting electrolyte) with simulated aerobic flue gas (18.5% CO_2, 3% O_2, N_2 balance) at a rate of 2 sccm, with the headspace CO_2 concentration measured from the gas outlet of the solution. Adapted with permission from ref 160. Copyright 2005 Springer Nature.

undergo disproportionation to form Mebipy$^+$ and Mebipy$^-$. The latter reacts with CO_2 to form Mebipy-CO_2^-, which results in a disappearance of the more cathodic redox event. The CO_2 adduct can then be electrochemically oxidized by two electrons to return the parent Mebipy$^+$ cation. For these monoalkylated bipyridinium species, the stoichiometry thus requires two electrons to capture one molecule of CO_2 due to the disproportionation event that occurs.

Buttry and co-workers also studied the related nonalkylated compound, 4,4′-bipyridine (bipy).[133] The one electron reduction of bipy produces the radical anion, bipy$^{\bullet-}$, which quickly binds to CO_2. Following oxidation of the bipy−$CO_2^{\bullet-}$ adduct, CO_2 is released and bipy is regenerated. This mechanism differs from the monoalkylated bipyridinium compounds. One equivalent of electrons is sufficient for capturing a single equivalent of CO_2 due to the more nucleophilic radical anion, which readily binds to CO_2 after a single reduction. In the ionic liquid *N*-butyl-*N*-methylpyrrolidinium bis(trifluoromethylsulfonyl)imide (BMF TFSI) under a N_2 atmosphere, reduction of bipy to bipy$^{\bullet-}$ is a one electron reversible couple at −2.25 V vs ferrocene. In a solution saturated with CO_2, the reduction peak for bipy$^{\bullet-}$ shifts from −2.3 V to −2.05 V vs ferrocene displaying strong binding between bipy$^{\bullet-}$ and CO_2. The bipy−$CO_2^{\bullet-}$ compound is oxidized at −1.35 V vs ferrocene, a substantial positive shift due to the very stable N−C bond formed in the adduct. The large potential difference between reduction and oxidation of this adduct is a crucial component as it can impact the total energy for the bipy−CO_2 capture/release cycle.

Computations were also carried out to elucidate the reaction mechanism of CO_2 capture by 4,4′-bipyridine.[133] Utilizing DFT (B3LYP and M062X) with the implicit continuum solvation model, the computations revealed that a stable adduct is formed between the 4,4′-bipyridine anion radical and the CO_2 molecule, with ΔG_0 = −43.9 kJ/mol. The release of the CO_2 molecule was then accomplished by reoxidation of the adduct, presumably yielding a zwitterionic intermediate, which is susceptible to a facile decarboxylation.

Recently, Li and co-workers reported the utilization of substituted pyridine derivatives as eCCC redox carriers.[161] A wide range of pyridines, phenazines, and azobenzene/pyridines were investigated primarily using cyclic voltammetry and DFT. Each of the latter investigated compounds reversibly binds two equivalents of CO_2 *via* an ECEC mechanism. CO_2 binding and release studies were performed with the most promising candidate, 4,4′-azopyridine, using a flow cell setup. The system had excellent cyclability, capturing CO_2 from 15 to 18.5% streams while maintaining ∼90% Faradaic efficiency over 20 capture/release cycles, even in the presence of 3−5% O_2 (Figure 10). During each cycle, the CO_2 concentration dropped to ∼10% during capture, and rose to ∼25% during release while continuously sparging the solution with 18.5% CO_2 (3% O_2 with N_2 balance, Figure 10). The authors determined the experimental energy consumption to be 120 kJ/mol, which corresponds to ∼3% energetic efficiency (based on a theoretical requirement of 4.18 kJ/mol for an 18.5−100% concentration swing). The flow cell setup used for the cycling studies was not optimized, however, which led to significant energetic losses. The authors estimate that the energetic efficiency can be increased with improved cell design (to ∼9% efficiency) to bring the energy consumption down to ∼48 kJ/mol (based on a ΔE of 500 mV between capture and release with the azopyridine system observed *via* cyclic voltammetry).

https://doi.org/10.1021/acs.chemrev.2c00681
Chem. Rev. 2023, 123, 8069−8098

5.2.4. Dithiols. Buttry and co-workers also described the use of thiolates as redox carriers.[134] Prior to this study, there were few reports of S-bound terminal thiocarbonates, and no description of the electrochemical behavior of thiocarbonate.[162,163] Buttry and co-workers specifically looked at benzyldisulfide (BDS) for direct eCCC, where they observed that from one equivalent of BDS, a two-electron reduction results in two equivalents of nucleophilic benzylthiolate that can react with one CO_2 molecule forming a *S*-benzylthiocarbonate (Scheme 7). Using DFT (B3LYP), CO_2 capture is

Scheme 7. Mechanism of CO_2 Capture *via* Reduction of Benzyldisulfide

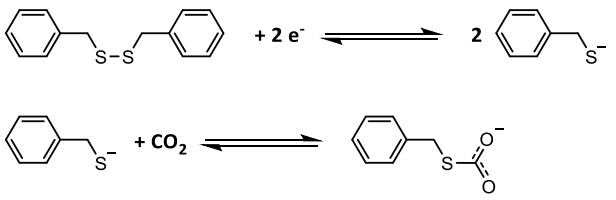

estimated to have a binding energy of −66 kJ mol^{-1}. Computations were also used to elucidate the CO_2 release step. The authors proposed that CO_2 release should follow the oxidation of thiocarbonate due to a significant electron density localized at the S−C bond of thiol and CO_2 in the redox-active molecular orbital (RAMO). Removing the electron from RAMO upon oxidation should thus lead to bond destabilization and rapid CO_2 release. From the overall mechanism, a stoichiometry of one CO_2 captured per one electron transferred to BDS was found, which theoretically allows for capture of two CO_2 molecules per each BDS.

Harris and Bushnell added to the BDS study from Buttry and co-workers using DFT to assess solvent effects while also exploring the use of other benzyldichalcogenide compounds.[164] Pursuant to the dielectric constant of different solvents, the absolute reduction potential and the interaction energy for benzylthiolate−CO_2 binding were exhibited to range between 2.7 and 3.4 V and −30 to −40 kJ/mol, respectively. They also found that the chalcogenide atom significantly impacted the oxidation/CO_2 release step. The CO_2 adducts formed in systems involving benzyldiselenide and benzylditelluride had less positive absolute reduction potentials compared to benzyldisulfide (BDS). Thus, the authors suggested using benzylditelluride and benzyldiselenide as the potential eCCC agents, as they should have a better peak-to-peak separation between the CO_2 capture and CO_2 release potentials. However, other factors, such as toxicity and availability, must also be considered.

5.3. Cell and System Design

Similar to the other eCCC approaches (i.e., pH-swing and EMAR), cell and system engineering will be critical in optimizing overall performance. To date, most studies employing redox-active capture molecules for direct eCCC have consisted of proof-of-concept, cyclic voltammetry, and/or bulk electrolysis experiments focused on characterizing capture species−electrolyte pairs in well-defined and controlled environments. Only a few studies have incorporated these molecules into an engineered cell design with flowing gas streams. Here, we describe lab-scale, engineered cells that have been employed in prior work, provide important operating conditions/performance indicators, and highlight key challenges regarding system design to motivate future work. A more thorough discussion on important system properties for direct eCCC approaches can be found in the review by Liu *et al.*, specifically for continuous processes with flowing electrolytes.[82]

In the electro-swing absorption (ESA) system previously introduced,[148,149] the redox-active capture agent is immobilized on the surface of a porous electrode. A counter electrode was used to complete the flow of electrons (Figure 8). Between both electrodes is a membrane/separator imbibed with the liquid electrolyte, which wets the porous electrodes with a liquid film. This facilitates the flow of ionic current between the electrodes and to the electrochemical reaction sites at the wetted electrode surface. During operation, the capture agent is activated *via* polarization and exposed to CO_2 for the capture step. Once the negative electrode is saturated with CO_2 the polarity of the cell is deliberately reversed, deactivating the capture agent at the now positive electrode to release CO_2 by desorption. In a flowing gas operation scheme, the feed gas containing CO_2 is fed to the working electrode through a parallel flow field, and thus CO_2 must diffuse laterally through both the porous media and the liquid film to react with the activated quinone species. For this system, cell operation is likely to be controlled by the CO_2 mass transfer rate through the porous electrode and liquid film, which may be orders of magnitude lower than both the electrochemical and chemical (binding and release) reaction rates. Accordingly, demonstrations for ESA systems have been limited to low current density operation ($\lesssim$2 mA cm^{-2}).[149] Additionally, it has been shown both experimentally and computationally that quinone utilization in a given cycle length is strongly dependent on the CO_2 concentration in the feed gas, which affects the driving force for film diffusion.[148]

For liquid-based capture molecules, testing in an engineered flow cell system has been more limited. Diederichsen *et al.* tested their liquid quinone chemistry in a redox flow battery type system, similar to what was described for some of the pH-swing setups in section 3.3 (and depicted in Figure 4).[156] Their cell comprised of interdigitated flow fields, carbon felt electrodes, and a Nafion 212 cation exchange membrane. The external electrolyte reservoirs, where CO_2 absorption and desorption were conducted, also contained plastic beads to increase the gas−liquid contact area and decrease mixing time. The cell was operated at constant current (10 mA) with rest periods between cycles (and a period of constant potential at the end of each oxidation step). The electrolyte contained ∼1 M quinone and was circulated through the cell at a flow rate of 1 mL min^{-1}, lower than previous demonstrations that have been discussed. When operated with a 15% CO_2 feed gas, the measured CO_2 capacity was ∼70% of its theoretical value; they hypothesize that these losses are due to insufficient flow patterns throughout the carbon felt electrodes. The capacity slightly decayed over 10 cycles, which they reason could have been caused by species crossover. Diederichsen *et al.* also developed a continuous flowing electrolyte system to test their liquid quinone (albeit at a 0.5 M concentration). The platform employed two flow cells to reduce (i.e., activate) and oxidize (i.e., deactivate) the quinone, where each cell used a ferrocene counter chemistry. Given that the system was operated continuously, even lower liquid flow rates were used (0.25−0.5 mL min^{-1}) to enable sufficient conversion rates with currents in the range of 10−35 mA. As described in section 5.2.1, the cells operated with energy requirements in the range

https://doi.org/10.1021/acs.chemrev.2c00681
Chem. Rev. 2023, 123, 8069−8098

of 35−220 kJ/mol CO_2; however, their tests in the continuous system only considered capture from a pure CO_2 stream.

5.4. Experimental Methods for Measuring CO_2 Binding Affinities

As described previously in section 5.1, the CO_2 binding affinity of the reduced and oxidized forms of the capture species ($K_{1(R^{n-})}$ and $K_{2(R)}$, respectively) must be optimized to enable sufficient CO_2 capture and release, respectively. Thus, determination of $K_{1(R^{n-})}$ and $K_{2(R)}$ values for the active and resting states of redox carriers is important. There are several methods used to measure binding coefficients; however, unique to redox carriers, electrochemical methods specific to the reaction mechanism can be employed to measure these equilibrium constants. For a system that employs an EC mechanism (electron transfer followed by chemical step), or EEC mechanism (where a chemical step follows two electron transfer steps), carrier-CO_2 binding constants (for $K_{1(R^{n-})}$ values between 100 and 10^{15}) can be measured using the observed shift in the half-wave potential, $E_{1/2}$, recorded in the presence and absence of a known concentration of CO_2 by applying eq 11.[129,165]

$$E_{1/2} = E^{o'} + \frac{RT}{nF}\ln(K_{1(R^{n-})}) + q\frac{RT}{nF}\ln[CO_2] \quad (11)$$

In the above equation, R is the universal gas constant, T is temperature, F is Faraday's constant, and n is the number of electrons being passed in the redox event. The number of CO_2 molecules that are bound during the chemical step is represented by the term q (which can be determined *via* other spectroscopic or voltammetric techniques[52,123,166]). $E^{o'}$ is the half-wave potential in the absence of CO_2, while $E_{1/2}$ represents the half-wave potential in the presence of a known CO_2 concentration in solution ($[CO_2]$). This approach can be highly beneficial as it does not require isolation of the active state carrier, which can often be unstable or difficult to isolate cleanly. For an EC mechanism where $K_{1(R^{n-})}$ values are larger than 10^{15}, the change in potential can be measured using the open circuit potential, with a varied range of CO_2 concentrations. In this case, the active state carrier must be formed chemically or electrochemically. The $E_{1/2}$ value from eq 11 would refer to the open circuit potential under a known concentration of CO_2. The $E^{o'}$ value would refer to the open circuit potential in the absence of CO_2. The y-intercept of the linear relationship of the change in open circuit potential versus the natural log of the concentration of CO_2 in solution can be used to find the binding constant. Values of $K_{1(R^{n-})}$ for redox carriers can also be determined using more common spectroscopic or physical techniques, depending on the magnitude of $K_{1(R^{n-})}$ and solubility of the carrier. These techniques include, but are not limited to NMR, electronic absorption spectroscopy, gravimetry, and gas uptake experiments.[52,123,167,168] An example of one of these methods is measuring the electronic absorption spectrum of an eCCC carrier under various concentrations of CO_2.[123] In order to utilize this method, however, the active state carrier must be used, meaning that it must be isolable and stable over the course of the experiments. The resulting spectra can be analyzed using a variety of approaches to assess the equilibrium constant, for example the Benesi−Hildebrand method.[169]

6. CONCLUDING REMARKS AND OUTLOOK

The use of electrochemical CO_2 capture and concentration was initially reported in literature in the 1960s. Since then, several different concepts and system architectures have been proposed, with significant advancements occurring over the past decade. Some of these systems already operate in the laboratory setting with estimated energetic efficiencies rivaling state-of-the-art systems. These results have demonstrated the promise of eCCC, but also outline scientific challenges that, if addressed, would accelerate implementation and widespread use.

(1) Long-term stability still represents a challenge in most eCCC systems. Most pH-swing, EMAR, and redox carrier systems are specifically sensitive to oxygen, which is commonly present in dilute CO_2 streams. A combination of modifying these systems to work at milder electrochemical potentials and implementing engineering design approaches (e.g., preseparating O_2 or water vapor from the inlet streams) could be used to address current issues surrounding instability in the presence of O_2 and/or water vapor (for nonaqueous systems). The stability of current chemistries toward other components in CO_2-containing streams (e.g., sulfur oxides, nitrous oxides, etc.) is also not clear and should be investigated in future work.

(2) Most studies have focused on improving the chemistry of eCCC systems, such as the carrier species and electrolyte, for proof-of-concept experiments. However, design and operation of the electrochemical cell will also greatly impact system performance. Characterization of overpotentials (e.g., mass transport, activation, ohmics) will be important for identifying key energy losses and guiding future design strategies for efficient systems. Additionally, further understanding of the interfacial (liquid−solid or gas−liquid−solid) phenomena will be necessary to enable high performance cell and electrode designs. Specifically, the use of nonaqueous solvents (as has been typical in direct eCCC systems) may require substantial studies into interfacial behavior and its impact on cell/system operation. Other aspects of cell performance, such as the occurrence of side reactions and species crossover, should also be considered. Gaining a further understanding of operating limitations can help guide the selection of optimal cell components (electrodes, membrane/separator, flow channels) and operating conditions.

(3) In general, researchers in the field have used a variety of experimental systems and reported observed performance with different indicators. Developing standardized platforms, experimental methods, and performance metrics can enable better comparisons across reported capture systems.

(4) Theoretical (quantum chemical) calculations have become an important tool in molecular design, but there are still several challenges associated with their use in large-scale industrial applications. The following highlight some of the major problems faced in theoretical calculations: (a) the high computational costs of quantum chemical calculations make it difficult to investigate a large enough space of potential molecular candidates, especially when a large number of calculations are required, (b) inadequate description

https://doi.org/10.1021/acs.chemrev.2c00681
Chem. Rev. 2023, 123, 8069−8098

of the models investigated in theoretical calculations can lead to inaccurate results. We recognize the major limitations of the theoretical models in the description of solvation, which can significantly impact the accuracy of the results, and (c) the lack of experimental data for validation of theoretical calculations is a major challenge, making it difficult to assess the reliability of the computed results.

(5) The required performance of eCCC to enable system costs that are competitive with (or better than) state of the art capture processes is currently unknown. Technoeconomic analyses could define performance requirements (e.g., energy use, performance decay rates) as well as inform material property sets and process/cell operating conditions that can enable cost competitive eCCC systems.

Interest in more efficient and scalable eCCC has been motivated by the urgency to develop technologies capable of capturing CO_2 both from power plant/industrial point sources to achieve minimal or no carbon emissions as well as directly from the air to reach net-negative carbon emissions.

NOTES

Throughout this review, we use the phrase "simulated flue gas" to indicate gas mixtures that were used in experiments which contain CO_2 concentrations representative of power plant flue gas (3−15% CO_2).[17,170] In addition to CO_2, the "simulated flue gas" mixtures in works referenced here contain a carrier gas (typically N_2) and may also contain additional flue gas components at relevant concentrations (such as O_2).

The maximum Faradaic efficiency expression in eq 9 was derived using equations shown by Clarke *et al.*[125] The following assumptions were made to yield the η_{Faradaic} expression: (1) solutions and gas mixtures are ideal, (2) the capture species is fully reduced/oxidized before absorption/desorption, (3) chemical equilibrium is achieved during absorption/desorption and is characterized by the binding coefficients $K_{1(R^{n-})} = \{[R(CO_2)_q^{n-}]\}/\{[R^{n-}][CO_2]^q\}$ and $K_{2(R)} = [R(CO_2)_q]/\{[R][CO_2]^q\}$, and (4) phase equilibrium is achieved during absorption/desorption such that dissolved CO_2 concentrations are represented with Henry's law. The derivation for η_{Faradaic} is outlined below:

$$\eta_{\text{Faradaic}} = \frac{\text{mol CO}_2\text{ separated}}{\text{mol e}^-\text{ transferred}} = \frac{\text{mol CO}_2\text{ separated per liter electrolyte}}{\text{mol e}^-\text{ transferred per liter electrolyte}}$$

moles of CO_2 separated can be determined from the difference between the maximum amount of CO_2 in solution following the absorption step (bound to R^{2-} and physically absorbed) and the amount of CO_2 leftover in solution (bound to R and physically absorbed) following the desorption step.

- mol CO_2 separated per liter of electrolyte =

$$(q[R(CO_2)_q^{n-}] + K_H P_i)_{\text{after absorption}} - (q[R(CO_2)_q] + K_H P_i)_{\text{after desorption}}$$

- after absorption:

$$[R]_T = [R(CO_2)_q^{n-}] + [R^{n-}] = [R(CO_2)_q^{n-}] + \frac{[R(CO_2)_q^{n-}]}{K_{1(R^{n-})}[CO_2]^q}$$

where $[CO_2] = K_H P_i$

- after desorption:

$$[R]_T = [R(CO_2)_q] + [R] = [R(CO_2)_q] + \frac{[R(CO_2)_q]}{K_{2(R)}[CO_2]^q}$$

where $[CO_2] = K_H P_f$

- mol CO_2 separated per liter of electrolyte =

$$\left(q[R]_T \frac{K_{1(R^{n-})}(K_H P_i)^q}{1 + K_{1(R^{n-})}(K_H P_i)^q} + K_H P_i\right) - \left(q[R]_T \frac{K_{2(R)}(K_H P_f)^q}{1 + K_{2(R)}(K_H P_f)^q} + K_H P_f\right)$$

moles of e^- transferred can be determined from the total capture species concentration.

- mol e^- transferred per liter electrolyte = $n[R]_T$

Plugging the derived expressions for "mol CO_2 separated per liter electrolyte" and "mol e^- transferred per liter electrolyte" yields eq 9 for η_{Faradaic}.

Table 2 compares measured CO_2 solubilities in aprotic solvents that are commonly used for electrochemical CO_2 separation systems.

Table 2. CO_2 Solubilities in Common Aprotic Solvents[124]

solvent	CO_2 solubility (mol/L atm)
acetonitrile	0.28
N,*N*-dimethylformamide	0.175
dimethylsulfoxide	0.135
propylene carbonate	0.129

AUTHOR INFORMATION

Corresponding Authors

Anastassia N. Alexandrova − *Department of Chemistry and Biochemistry, University of California, Los Angeles, Los Angeles, California 90095-1569, United States;* orcid.org/0000-0002-3003-1911; Email: ana@chem.ucla.edu

Fikile R. Brushett − *Department of Chemical Engineering, Massachusetts Institute of Technology, Cambridge, Massachusetts 02142, United States;* orcid.org/0000-0002-7361-6637; Email: brushett@mit.edu

Jenny Y. Yang − *Department of Chemistry, University of California, Irvine, California 92697, United States;* orcid.org/0000-0002-9680-8260; Email: j.yang@uci.edu

Authors

Alessandra M. Zito − *Department of Chemistry, University of California, Irvine, California 92697, United States;* orcid.org/0000-0002-1111-5415

Lauren E. Clarke − *Department of Chemical Engineering, Massachusetts Institute of Technology, Cambridge, Massachusetts 02142, United States*

Jeffrey M. Barlow − *Department of Chemistry, University of California, Irvine, California 92697, United States*

Daniel Bím − *Department of Chemistry and Biochemistry, University of California, Los Angeles, Los Angeles, California 90095-1569, United States;* orcid.org/0000-0003-3100-4293

Zisheng Zhang − *Department of Chemistry and Biochemistry, University of California, Los Angeles, Los Angeles, California 90095-1569, United States;* orcid.org/0000-0002-4370-4038

https://doi.org/10.1021/acs.chemrev.2c00681
Chem. Rev. 2023, 123, 8069−8098

Katelyn M. Ripley − *Department of Chemical Engineering, Massachusetts Institute of Technology, Cambridge, Massachusetts 02142, United States*
Clarabella J. Li − *Department of Chemistry, University of California, Irvine, California 92697, United States*
Amanda Kummeth − *Department of Chemistry, University of California, Irvine, California 92697, United States*
McLain E. Leonard − *Department of Chemical Engineering, Massachusetts Institute of Technology, Cambridge, Massachusetts 02142, United States*

Complete contact information is available at: https://pubs.acs.org/10.1021/acs.chemrev.2c00681

Author Contributions

[‖]A.M.Z., L.E.C., J.M.B., and D.B. contributed equally. CRediT: **Alessandra M. Zito** data curation, formal analysis, investigation, methodology, writing-original draft; **Lauren E. Clarke** data curation, formal analysis, investigation, methodology, writing-original draft; **Jeffrey M. Barlow** data curation, formal analysis, investigation, methodology, writing-review & editing; **Daniel Bím** data curation, formal analysis, investigation, methodology, visualization, writing-original draft; **Zisheng Zhang** data curation, formal analysis, investigation, methodology, writing-original draft; **Katelyn M. Ripley** investigation, writing-review & editing; **Clarabella J. Li** investigation, writing-review & editing; **Amanda Kummeth** investigation, writing-review & editing; **McLain E. Leonard** investigation, writing-review & editing; **Anastassia N. Alexandrova** conceptualization, funding acquisition, resources, supervision, writing-review & editing; **Fikile R. Brushett** conceptualization, funding acquisition, resources, supervision, writing-review & editing; **Jenny Y. Yang** conceptualization, funding acquisition, resources, supervision, writing-review & editing.

Notes

The authors declare no competing financial interest.

Biographies

Alessandra M. Zito was born and raised in Broomall, PA. She received her Bachelor's degree in Chemistry from Johns Hopkins University, where she worked with Professor V. Sara Thoi, investigating catalyst loading on carbon aerogels and homogeneous CO_2 reduction catalysts. Alessandra is currently a Ph.D. candidate in the Department of Chemistry at UC Irvine, performing research in Professor Jenny Y. Yang's lab. In her work, she synthesizes and characterizes redox carriers for electrochemical carbon dioxide capture and concentration.

Lauren E. Clarke received her B.S. and M.S. in Chemical Engineering from the University of North Dakota in 2016 and 2018, respectively. She also obtained her M.S. in Chemical Engineering Practice in 2020 from the Massachusetts Institute of Technology (MIT). Lauren is currently a Ph.D. candidate in the Department of Chemical Engineering at MIT, performing research in Prof. Fikile R. Brushett's group. In her work, she uses a combination of modeling and experiments to understand the impact of material properties and operating parameters on the performance of electrochemical carbon dioxide separation systems.

Jeffrey M. Barlow was born and raised in Boise, Idaho. He received his Bachelor's degree in Chemistry from Boise State University, where he worked with Professor Eric C. Brown, investigating hydrogen-bonding interactions in synthetic mimics of carbonic anhydrase and ADA DNA repair protein. He then completed his doctoral studies at UC Irvine under Professor Jenny Y. Yang, where his research focused on the utilization of secondary interactions to promote energy efficient electrochemical approaches for CO_2 capture and conversion. He is currently a postdoctoral fellow at Argonne National Laboratory, investigating photochemical CO_2 capture and conversion under David Kaphan and David Tiede.

Daniel Bím is a researcher specializing in organic, inorganic, and bioinorganic catalysis and spectroscopy. He was born in Prague, Czech Republic, and received his Ph.D. from Charles University, where he conducted research on computational electrochemistry and reactivity of transition-metal complexes and metalloenzymes. As a postdoctoral researcher in the Prof. Alexandrova group at UCLA, he studied the influence of internal electric fields on enzymes catalysis. Currently, Daniel is a Marie Skłodowska-Curie Fellow at Caltech, performing interdisciplinary research focusing on understanding the mechanisms of photoredox catalysis by transition-metal complexes.

Zisheng Zhang was born in Wuhan, PRC. He received a B.Sc. in Chemistry from South University of Science and Technology of China in 2019 advised by Prof. Jun Li. At UCLA, he was a UCLA-CSST fellow in 2018, obtained a M.Sc. in Chemistry in 2021, and is currently a Ph.D. candidate advised by Prof. Anastassia N. Alexandrova. In summer, 2022, he worked with Dr. Maria K. Chan as a research intern at Argonne National Lab. His research interests include realistic modeling of catalytic interfaces and inverse design of functional molecules.

Katelyn M. Ripley received her B.S. and M.S. in Chemical Engineering and Engineering Management, respectively, from Northeastern University in 2020. She is currently a Ph.D. candidate and NDSEG fellow in Prof. Fikile R. Brushett's group in the Department of Chemical Engineering at MIT, where she has worked on both electrochemical carbon dioxide separation systems and high-temperature nonaqueous redox flow batteries. Her current research is focused on developing a techno-economic model for electrochemical CO_2 separation systems.

Clarabella J. Li received her B.S. in Chemistry with an emphasis in Forensics from UC Davis. At Davis, she worked with Prof. Mark J. Kurth synthesizing pharmaceutical compounds relevant to cystic fibrosis and developing methodology for nitrogen-containing heterocycles. Presently, she is a Ph.D. candidate in Chemistry at UC Irvine, studying under the mentorship of Prof. Jenny Y. Yang. Her current field of research is studying electrochemical systems for CO_2 capture.

Amanda Kummeth received a BA in Chemistry from Colgate University. She then escaped to warmer climates and got her MS in Chemistry from University of California Irvine, where she worked with Professor Jenny Yang, trying to capture and concentrate CO_2. Amanda currently is working as a research chemist in PPG's aerospace division.

McLain E. Leonard, Ph.D. is currently the Senior Electrochemical Engineer for Ebb Carbon, Inc., in San Carlos, CA. He received his Ph.D. in Chemical Engineering from the Massachusetts Institute of Technology in 2021 after completing a series of studies focused on electrochemical carbon dioxide utilization and capture technologies at the cell and component levels. He is presently working to commercialize a nascent approach to carbon dioxide capture and is a professional member of The Electrochemical Society.

Anastassia N. Alexandrova is a Professor in the Department of Chemistry and Biochemistry, UCLA. She obtained a B.S./M.S. Diploma with highest honors from Saratov University, Russia, her Ph.D. in Theoretical Physical Chemistry from Utah State University and was then a Postdoctoral Associate and an American Cancer Society Postdoctoral Fellow at Yale University. Anastassia joined the

https://doi.org/10.1021/acs.chemrev.2c00681
Chem. Rev. 2023, 123, 8069−8098

faculty of UCLA and CNSI in 2010. The focus of her laboratory is theory and computation for design and multiscale modeling of functional materials: dynamic catalytic interfaces, artificial metalloenzymes, molecular qubits and their assemblies, and quantum materials. She is a recipient of numerous awards, such as NSF CAREER Award, Sloan Fellowship 2013, DARPA Young Faculty Award 2011, Fulbright Fellowship 2016, and ACS WCC Rising Star Award 2016, 2020 ACS Phys Early Career Award in Theoretical Chemistry, 2021 Max Planck–Humboldt medal, as well as UCLA's Hanson–Dow award for excellence in teaching 2016, Herbert Newby McCoy award for excellence in faculty research 2016, undergraduate research mentorship award 2018, and 2019 Distinguished Teaching Award (the highest honor for teaching given in UCLA).

Fikile R. Brushett is an Associate Professor of Chemical Engineering at the Massachusetts Institute of Technology (MIT). Prior to joining MIT, he received his Ph.D. from the University of Illinois at Urbana–Champaign and was a Director's Postdoctoral Fellow at Argonne National Laboratory. He leads a research group advancing the science and engineering of electrochemical technologies for a sustainable energy economy. Their current efforts focus on redox flow batteries for grid storage and electrochemical processes for carbon management and chemical manufacturing. Brushett also serves as the Research Integration co-Lead for the Joint Center for Energy Storage Research, a DOE-funded energy innovation hub.

Jenny Y. Yang is a Professor of Chemistry at the University of California, Irvine (UCI). She received her B.S. degree in Chemistry at UC Berkeley, where she worked for Prof. Jeffry R. Long, and her Ph.D. with Prof. Daniel G. Nocera at MIT. She was a postdoctoral associate at the Pacific Northwest National Laboratory (PNNL) with Dr. Daniel L. DuBois. She continued as a scientist at PNNL and then at the Joint Center for Artificial Photosynthesis at Caltech before starting as an Assistant Professor at UCI. Her research is focused on inorganic catalysis and electrochemical processes relevant to small molecule activation and sustainability. She is currently director of the DOE-funded Center for Closing the Carbon Cycle.

ACKNOWLEDGMENTS

We thank the Sloan Foundation for funding the authors of this review. A.M.Z. gratefully acknowledges the support of the National Science Foundation Graduate Research Fellowship. K.M.R. gratefully acknowledges the support of the Department of Defense National Defense Science and Engineering Graduate (NDSEG) Fellowship.

REFERENCES

(1) *Climate Change 2022: Mitigation of Climate Change. Contribution of Working Group III to the Sixth Assessment Report of the Intergovernmental Panel on Climate Change*; Intergovernmental Panel on Climate Change: Cambridge, UK and New York, NY, 2022.
(2) *Global Energy Review: CO_2 Emissions in 2021*; Internional Energy Agency: Paris, 2022.
(3) Friedlingstein, P.; Jones, M. W.; O'Sullivan, M.; Andrew, R. M.; Bakker, D. C. E.; Hauck, J.; Le Quéré, C.; Peters, G. P.; Peters, W.; Pongratz, J.; et al. Global Carbon Budget 2021. *Earth Syst. Sci. Data* **2022**, *14* (4), 1917–2005.
(4) Rogelj, J.; den Elzen, M.; Höhne, N.; Fransen, T.; Fekete, H.; Winkler, H.; Schaeffer, R.; Sha, F.; Riahi, K.; Meinshausen, M. Paris Agreement Climate Proposals Need a Boost to Keep Warming Well below 2 °C. *Nature* **2016**, *534*, 631.
(5) *Net Zero by 2050*; International Energy Agency: Paris, 2021.
(6) Ritchie, H.; Roser, M.; Rosado, P. CO_2 and Greenhouse Gas Emissions. *Our World Data* **2020**.
(7) Metz, B.; Davidson, O.; de Coninck, H.; Loos, M.; Meyer, L. *IPCC Special Report on Carbon Dioxide Capture and Storage*; UK, Cambridge, 2005.
(8) Chu, S.; Majumdar, A. Opportunities and Challenges for a Sustainable Energy Future. *Nature* **2012**, *488*, 294.
(9) Lackner, K. S.; Brennan, S.; Matter, J. M.; Park, A. H. A.; Wright, A.; Van Der Zwaan, B. The Urgency of the Development of CO 2 Capture from Ambient Air. *Proc. Natl. Acad. Sci. U. S. A.* **2012**, *109* (33), 13156–13162.
(10) *Facilities Database*; Global CCS Institute, 2022; https://co2re.co/FacilityData (accessed 2022-09-01).
(11) Tavoni, M.; van der Zwaan, B. Nuclear Versus Coal plus CCS: A Comparison of Two Competitive Base-Load Climate Control Options. *Environ. Model. Assess.* **2011**, *16* (5), 431–440.
(12) *Direct Air Capture*; International Energy Agency: Paris, 2022.
(13) Hammond, G. P.; Akwe, O. S. O.; Williams, S. Techno-Economic Appraisal of Fossil-Fuelled Power Generation Systems with Carbon Dioxide Capture and Storage. *Energy* **2011**, *36* (2), 975–984.
(14) House, K. Z.; Baclig, A. C.; Ranjan, M.; Van Nierop, E. A.; Wilcox, J.; Herzog, H. J. Economic and Energetic Analysis of Capturing CO2 from Ambient Air. *Proc. Natl. Acad. Sci. U. S. A.* **2011**, *108* (51), 20428–20433.
(15) Chao, C.; Deng, Y.; Dewil, R.; Baeyens, J.; Fan, X. Post-Combustion Carbon Capture. *Renew. Sustain. Energy Rev.* **2021**, *138*, 110490.
(16) Raza, A.; Gholami, R.; Rezaee, R.; Rasouli, V.; Rabiei, M. Significant Aspects of Carbon Capture and Storage – A Review. *Petroleum* **2019**, *5* (4), 335–340.
(17) Wang, X.; Song, C. Carbon Capture From Flue Gas and the Atmosphere: A Perspective. *Front. Energy Res.* **2020**, *8*, 560849.
(18) Yu, C. H.; Huang, C. H.; Tan, C. S. A Review of CO2 Capture by Absorption and Adsorption. *Aerosol Air Qual. Res.* **2012**, *12* (5), 745–769.
(19) House, K. Z.; Harvey, C. F.; Aziz, M. J.; Schrag, D. P. The Energy Penalty of Post-Combustion CO2 Capture & Storage and Its Implications for Retrofitting the U.S. Installed Base. *Energy Environ. Sci.* **2009**, *2*, 193.
(20) Abu-Zahra, M. R. M.; Schneiders, L. H. J.; Niederer, J. P. M.; Feron, P. H. M.; Versteeg, G. F. CO2 Capture from Power Plants: Part I. A Parametric Study of the Technical Performance Based on Monoethanolamine. *Int. J. Greenh. Gas Control* **2007**, *1* (1), 37–46.
(21) Goto, K.; Kodama, S.; Okabe, H.; Fujioka, Y. Energy Performance of New Amine-Based Solvents for CO2 Capture from Blast Furnace Gas. *ACS Symp. Ser.* **2012**, *1097*, 317.
(22) Singh, A.; Stéphenne, K. Shell Cansolv CO2 Capture Technology: Achievement from First Commercial Plant. *Energy Procedia* **2014**, *63*, 1678–1685.
(23) Yulia, F.; Sofianita, R.; Prayogo, K.; Nasruddin, N. Optimization of Post Combustion CO2 Absorption System Monoethanolamine (MEA) Based for 320 MW Coal-Fired Power Plant Application – Exergy and Exergoenvironmental Analysis. *Case Stud. Therm. Eng.* **2021**, *26*, No. 101093.
(24) Rochelle, G.; Chen, E.; Freeman, S.; Van Wagener, D.; Xu, Q.; Voice, A. Aqueous Piperazine as the New Standard for CO2 Capture Technology. *Chem. Eng. J.* **2011**, *171* (3), 725–733.
(25) Boot-Handford, M. E.; Abanades, J. C.; Anthony, E. J.; Blunt, M. J.; Brandani, S.; Mac Dowell, N.; Fernández, J. R.; Ferrari, M. C.; Gross, R.; Hallett, J. P.; et al. Carbon Capture and Storage Update. *Energy Environ. Sci.* **2014**, *7* (1), 130–189.
(26) Rochelle, G. T. Amine Scrubbing for CO2 Capture. *Science (80-.)* **2009**, *325* (5948), 1652–1654.
(27) Wilcox, J. *Carbon Capture*; Springer: New York, 2012.
(28) Mirza, N.; Kearns, D. In *State of the Art: CCS Tchnologies*; Global CCS Institute, 2022.
(29) Baylin-Stern, A.; Berghout, N. *Is carbon capture too expensive? Analysis*; International Energy Agency, 2023; https://www.iea.org/commentaries/is-carbon-capture-too-expensive (accessed 2023-02-21).

https://doi.org/10.1021/acs.chemrev.2c00681
Chem. Rev. 2023, 123, 8069–8098

(30) Fasihi, M.; Efimova, O.; Breyer, C. Techno-Economic Assessment of CO2 Direct Air Capture Plants. *J. Clean. Prod.* **2019**, *224*, 957−980.
(31) Mcqueen, N.; Psarras, P.; Ne, H.; Pilorgé, P.; Liguori, S.; He, J.; Yuan, M.; Woodall, C. M.; Kian, K.; Pierpoint, L.; et al. Cost Analysis of Direct Air Capture and Sequestration Coupled to Low-Carbon Thermal Energy in the United States. *Environ. Sci. Technol.* **2020**, *54*, 7542.
(32) Lackner, K. S.; Azarabadi, H. Buying down the Cost of Direct Air Capture. *Ind. Eng. Chem. Res.* **2021**, *60* (22), 8196−8208.
(33) Page, B.; Turan, G.; Zapantis, A.; Beck, L.; Consoli, C.; Havercroft, I.; Liu, H.; Loria, P.; Schneider, A.; Tamme, E. *Global Status of CCS 2019: Targeting*; Institute of Gas Engineers and Managers, 2019.
(34) Lackner, K. S. The Thermodynamics of Direct Air Capture of Carbon Dioxide. *Energy* **2013**, *50* (1), 38−46.
(35) Stern, M. C.; Simeon, F.; Herzog, H.; Hatton, T. A. Post-Combustion Carbon Dioxide Capture Using Electrochemically Mediated Amine Regeneration. *Energy Environ. Sci.* **2013**, *6*, 2505.
(36) Stern, M. C.; Simeon, F.; Hammer, T.; Landes, H.; Herzog, H. J.; Hatton, T. A. Electrochemically Mediated Separation for Carbon Capture. *Energy Procedia* **2011**, *4*, 860−867.
(37) Shaw, R. A.; Hatton, T. A. Electrochemical CO2 Capture Thermodynamics. *Int. J. Greenhouse Gas Control* **2020**, *95*, No. 102878.
(38) Rheinhardt, J. H.; Singh, P.; Tarakeshwar, P.; Buttry, D. A. Electrochemical Capture and Release of Carbon Dioxide. *ACS Energy Lett.* **2017**, *2* (2), 454−461.
(39) Barlow, J. M.; Clarke, L. E.; Zhang, Z.; Bím, D.; Ripley, K. M.; Zito, A.; Brushett, F. R.; Alexandrova, A. N.; Yang, J. Y. Molecular Design of Redox Carriers for Electrochemical CO2 Capture and Concentration. *Chem. Soc. Rev.* **2022**, *51* (20), 8415−8433.
(40) Huebscher, R. G.; Babinsky, A. D. Electrochemical Concentration and Separation of Carbon Dioxide for Advanced Life Support Systems - Carbonation Cell System. *SAE Techn. Pap.* **1969**, 690640.
(41) Dell'Osso, L.; Ruder, J. M.; Winnick, J. Mixed-Gas Adsorption and Vacuum Desorption of Carbon Dioxide on Molecular Sieve. Bed Performance and Data Analysis. *Ind. Eng. Chem. Process Des. Dev.* **1969**, *8* (4), 477−482.
(42) Martin, R. B. Carbon Dioxide Control for Manned Spacecraft. *Aerosp. Med.* **1968**, *39*, 937−941.
(43) Quattrone, P. D.; Wynveen, R. A. Electrochemical Carbon Dioxide Concentrating System. In *Life Support and Environmental Control Conference*, 1971.
(44) Wynveen, R. A.; Schubert, F. H.; Powell, J. D. *One-Man, Self-Contained CO2 Concentrating System*, 1972.
(45) Winnick, J.; Marshall, R. D.; Schubert, F. H. An Electrochemical Device for Carbon Dioxide Concentration, i. System Design and Performance. *Ind. Eng. Chem. Process Des. Dev.* **1974**, *13* (1), 59−63.
(46) Eisaman, M. D.; Schwartz, D. E.; Amic, S.; Larner, D.; Zesch, J.; Torres, F.; Littau, K. Energy-Efficient Electrochemical CO2 Capture from the Atmosphere. *Clean Technol.* **2009**, *2009*, 175−178.
(47) Winnick, J.; Toghiani, H.; Quattrone, P. D. Carbon Dioxide Concentration for Manned Spacecraf Using a Molten Carbonate Electrochemical Cell. *AlChE J.* **1982**, *28* (1), 103−111.
(48) Weaver, J. L.; Winnick, J. The Molten Carbonate Carbon Dioxide Concentrator: Cathode Performance at High CO2 Utilization. *J. Electrochem. Soc.* **1983**, *130* (1), 20−28.
(49) Kang, M. P.; Winnick, J. Concentration of Carbon Dioxide by a High-Temperature Electrochemical Membrane Cell. *J. Appl. Electrochem.* **1985**, *15* (3), 431−439.
(50) Eisaman, M. D.; Alvarado, L.; Larner, D.; Wang, P.; Garg, B.; Littau, K. A. CO2 Separation Using Bipolar Membrane Electrodialysis. *Energy Environ. Sci.* **2011**, *4*, 1319−1328.
(51) Watkins, J. D.; Siefert, N. S.; Zhou, X.; Myers, C. R.; Kitchin, J. R.; Hopkinson, D. P.; Nulwala, H. B. Redox-Mediated Separation of Carbon Dioxide from Flue Gas. *Energy Fuels* **2015**, *29* (11), 7508−7515.
(52) Bell, W. L.; Miedaner, A.; Smart, J. C.; DuBois, D. L. Synthesis and Evaluation of Electroactive CO2 Carriers. *SAE Techn. Pap.* **1988**, 881078.
(53) Jiang, L.; Roskilly, A. P.; Wang, R. Z. Performance Exploration of Temperature Swing Adsorption Technology for Carbon Dioxide Capture. *Energy Convers. Manag.* **2018**, *165*, 396−404.
(54) Bahamon, D.; Díaz-Márquez, A.; Gamallo, P.; Vega, L. F. Energetic Evaluation of Swing Adsorption Processes for CO2 Capture in Selected MOFs and Zeolites: Effect of Impurities. *Chem. Eng. J.* **2018**, *342*, 458−473.
(55) Sharifian, R.; Wagterveld, R. M.; Digdaya, I. A.; Xiang, C.; Vermaas, D. A. Electrochemical Carbon Dioxide Capture to Close the Carbon Cycle. *Energy Environ. Sci.* **2021**, *14* (2), 781−814.
(56) Ye, W.; Huang, J.; Lin, J.; Zhang, X.; Shen, J.; Luis, P.; Van Der Bruggen, B. Environmental Evaluation of Bipolar Membrane Electrodialysis for NaOH Production from Wastewater: Conditioning NaOH as a CO2 Absorbent. *Sep. Purif. Technol.* **2015**, *144*, 206−214.
(57) Eisaman, M. D.; Alvarado, L.; Larner, D.; Wang, P.; Littau, K. A. CO2 Desorption Using High-Pressure Bipolar Membrane Electrodialysis. *Energy Environ. Sci.* **2011**, *4* (10), 4031−4037.
(58) Sabatino, F.; Mehta, M.; Grimm, A.; Gazzani, M.; Gallucci, F.; Kramer, G. J.; Van Sint Annaland, M. Evaluation of a Direct Air Capture Process Combining Wet Scrubbing and Bipolar Membrane Electrodialysis. *Ind. Eng. Chem. Res.* **2020**, *59* (15), 7007−7020.
(59) Datta, S.; Henry, M. P.; Lin, Y. J.; Fracaro, A. T.; Millard, C. S.; Snyder, S. W.; Stiles, R. L.; Shah, J.; Yuan, J.; Wesoloski, L.; et al. Electrochemical CO2 Capture Using Resin-Wafer Electrodeionization. *Ind. Eng. Chem. Res.* **2013**, *52*, 15177.
(60) Eisaman, M. D.; Parajuly, K.; Tuganov, A.; Eldershaw, C.; Chang, N.; Littau, K. A. CO2 Extraction from Seawater Using Bipolar Membrane Electrodialysis. *Energy Environ. Sci.* **2012**, *5* (6), 7346−7352.
(61) Digdaya, I. A.; Sullivan, I.; Lin, M.; Han, L.; Cheng, W. H.; Atwater, H. A.; Xiang, C. A Direct Coupled Electrochemical System for Capture and Conversion of CO2 from Oceanwater. *Nat. Commun.* **2020**, *11* (1), 1−10.
(62) Warren, J. J.; Tronic, T. A.; Mayer, J. M. Thermochemistry of Proton-Coupled Electron Transfer Reagents and Its Implications. *Chem. Rev.* **2010**, *110*, 6961.
(63) Winsberg, J.; Hagemann, T.; Janoschka, T.; Hager, M. D.; Schubert, U. S. Redox-Flow Batteries: From Metals to Organic Redox-Active Materials. *Angew. Chemie Int. Ed.* **2017**, *56* (3), 686−711.
(64) Huang, C.; Liu, C.; Wu, K.; Yue, H.; Tang, S.; Lu, H.; Liang, B. CO2 Capture from Flue Gas Using an Electrochemically Reversible Hydroquinone/Quinone Solution. *Energy Fuels* **2019**, *33* (4), 3380−3389.
(65) Huynh, M. T.; Anson, C. W.; Cavell, A. C.; Stahl, S. S.; Hammes-Schiffer, S. Quinone 1 E- and 2 e-/2 H+ Reduction Potentials: Identification and Analysis of Deviations from Systematic Scaling Relationships. *J. Am. Chem. Soc.* **2016**, *138* (49), 15903−15910.
(66) Yang, B.; Hoober-Burkhardt, L.; Krishnamoorthy, S.; Murali, A.; Prakash, G. K. S.; Narayanan, S. R. High-Performance Aqueous Organic Flow Battery with Quinone-Based Redox Couples at Both Electrodes. *J. Electrochem. Soc.* **2016**, *163* (7), A1442−A1449.
(67) Lin, K.; Gómez-Bombarelli, R.; Beh, E. S.; Tong, L.; Chen, Q.; Valle, A.; Aspuru-Guzik, A.; Aziz, M. J.; Gordon, R. G. A Redox-Flow Battery with an Alloxazine-Based Organic Electrolyte. *Nat. Energy* **2016**, *1* (9), 1−8.
(68) Lin, K.; Chen, Q.; Gerhardt, M. R.; Tong, L.; Kim, S. B.; Eisenach, L.; Valle, A. W.; Hardee, D.; Gordon, R. G.; Aziz, M. J.; et al. Alkaline Quinone Flow Battery. *Science (80-.)* **2015**, *349* (6255), 1529−1532.
(69) Er, S.; Suh, C.; Marshak, M. P.; Aspuru-Guzik, A. Computational Design of Molecules for an All-Quinone Redox Flow Battery. *Chem. Sci.* **2015**, *6* (2), 885−893.
(70) Jin, S.; Wu, M.; Gordon, R. G.; Aziz, M. J.; Kwabi, D. G. PH Swing Cycle for CO2 Capture Electrochemically Driven through

https://doi.org/10.1021/acs.chemrev.2c00681
Chem. Rev. 2023, 123, 8069−8098

Proton-Coupled Electron Transfer. *Energy Environ. Sci.* **2020**, *13* (10), 3706−3722.
(71) Xie, H.; Wu, Y.; Liu, T.; Wang, F.; Chen, B.; Liang, B. Low-Energy-Consumption Electrochemical CO2 Capture Driven by Biomimetic Phenazine Derivatives Redox Medium. *Appl. Energy* **2020**, *259*, 114119.
(72) Jin, S.; Wu, M.; Jing, Y.; Gordon, R. G.; Aziz, M. J. Low Energy Carbon Capture via Electrochemically Induced PH Swing with Electrochemical Rebalancing. *Nat. Commun.* **2022**, *13*, 2140.
(73) Seo, H.; Rahimi, M.; Hatton, T. A. Electrochemical Carbon Dioxide Capture and Release with a Redox-Active Amine. *J. Am. Chem. Soc.* **2022**, *144* (5), 2164−2170.
(74) Yamaguchi, A.; Inuzuka, R.; Takashima, T.; Hayashi, T.; Hashimoto, K.; Nakamura, R. Regulating Proton-Coupled Electron Transfer for Efficient Water Splitting by Manganese Oxides at Neutral PH. *Nat. Commun.* **2014**, *5*, 4256.
(75) Rahimi, M.; Catalini, G.; Hariharan, S.; Wang, M.; Puccini, M.; Hatton, T. A. Carbon Dioxide Capture Using an Electrochemically Driven Proton Concentration Process. *Cell Reports Phys. Sci.* **2020**, *1* (4), No. 100033.
(76) Xie, H.; Jiang, W.; Liu, T.; Wu, Y.; Wang, Y.; Chen, B.; Niu, D.; Liang, B. Low-Energy Electrochemical Carbon Dioxide Capture Based on a Biological Redox Proton Carrier. *Cell Reports Phys. Sci.* **2020**, *1* (5), No. 100046.
(77) Costentin, C. Electrochemical Approach to the Mechanistic Study of Proton-Coupled Electron Transfer. *Chem. Rev.* **2008**, *108* (7), 2145−2179.
(78) Song, N.; Gagliardi, C. J.; Binstead, R. A.; Zhang, M. T.; Thorp, H.; Meyer, T. J. Role of Proton-Coupled Electron Transfer in the Redox Interconversion between Benzoquinone and Hydroquinone. *J. Am. Chem. Soc.* **2012**, *134* (45), 18538−18541.
(79) Kwabi, D. G.; Aziz, M. J.; John, H.; Paulson, A. PH Swing Cycle for CO2 Capture Electrochemically Driven through Proton-Coupled Electron Transfer. *ChemRxiv* 2019.
(80) Huskinson, B.; Marshak, M. P.; Suh, C.; Er, S.; Gerhardt, M. R.; Galvin, C. J.; Chen, X.; Aspuru-Guzik, A.; Gordon, R. G.; Aziz, M. J. A Metal-Free Organic-Inorganic Aqueous Flow Battery. *Nature* **2014**, *505*, 195−198.
(81) Rahimi, M.; Catalini, G.; Puccini, M.; Hatton, T. A. Bench-Scale Demonstration of CO2 Capture with an Electrochemically Driven Proton Concentration Process. *RSC Adv.* **2020**, *10* (29), 16832−16843.
(82) Liu, Y.; Lucas, É.; Sullivan, I.; Li, X.; Xiang, C. Challenges and Opportunities in Continuous Flow Processes for Electrochemically Mediated Carbon Capture. *iScience* **2022**, *25* (10), No. 105153.
(83) Leitz, F. B.; Marinčić, L. Enhanced Mass Transfer in Electrochemical Cells Using Turbulence Promoters. *J. Appl. Electrochem.* **1977**, *7* (6), 473−484.
(84) Mondal, M. K.; Balsora, H. K.; Varshney, P. Progress and Trends in CO2 Capture/Separation Technologies: A Review. *Energy* **2012**, *46* (1), 431−441.
(85) Wang, M.; Herzog, H. J.; Hatton, T. A. CO2 Capture Using Electrochemically Mediated Amine Regeneration. *Ind. Eng. Chem. Res.* **2020**, *59* (15), 7087−7096.
(86) Stern, M. Electrochemically Mediated Amine Regeneration for Carbon Dioxide Separations. Ph.D. Thesis. Massachusetts Institute of Technology, 2013.
(87) Wang, M.; Hariharan, S.; Shaw, R. A.; Hatton, T. A. Energetics of Electrochemically Mediated Amine Regeneration Process for Flue Gas CO2 Capture. *Int. J. Greenh. Gas Control* **2019**, *82*, 48−58.
(88) Stern, M. C.; Hatton, T. A. Bench-Scale Demonstration of CO2 Capture with Electrochemically-Mediated Amine Regeneration. *RSC Adv.* **2014**, *4*, 5906−5914.
(89) Wang, M.; Hatton, T. A. Flue Gas CO2 Capture via Electrochemically Mediated Amine Regeneration: Desorption Unit Design and Analysis. *Ind. Eng. Chem. Res.* **2020**, *59*, 10120−10129.
(90) Eltayeb, A. O.; Stern, M. C.; Herzog, H.; Hatton, T. A. Energetics of Electrochemically-Mediated Amine Regeneration. *Energy Procedia* **2014**, *63*, 595−604.
(91) Wang, M.; Rahimi, M.; Kumar, A.; Hariharan, S.; Choi, W.; Hatton, T. A. Flue Gas CO2 Capture via Electrochemically Mediated Amine Regeneration: System Design and Performance. *Appl. Energy* **2019**, *255*, 113879.
(92) Liu, G. X.; Yu, Y. S.; Hong, Y. T.; Zhang, Z. X.; Wei, J. J.; Wang, G. G. X. Identifying Electrochemical Effects in a Thermal−Electrochemical Co-Driven System for CO2 Capture. *Phys. Chem. Chem. Phys.* **2017**, *19* (20), 13230−13244.
(93) Eltayeb, A. Analysis and Design of Electrochemically Mediated Carbon Dioxide Separation. Ph.D. Thesis. Massachusetts Institute of Technology, 2017.
(94) Colli, A. N.; Toelzer, R.; Bergmann, M. E. H.; Bisang, J. M. Mass-Transfer Studies in an Electrochemical Reactor with a Small Interelectrode Gap. *Electrochim. Acta* **2013**, *100*, 78−84.
(95) Castañeda, L. F.; Walsh, F. C.; Nava, J. L.; Ponce de León, C. Graphite Felt as a Versatile Electrode Material: Properties, Reaction Environment, Performance and Applications. *Electrochim. Acta* **2017**, *258*, 1115−1139.
(96) Babic, U.; Suermann, M.; Büchi, F. N.; Gubler, L.; Schmidt, T. J. Critical Review—Identifying Critical Gaps for Polymer Electrolyte Water Electrolysis Development. *J. Electrochem. Soc.* **2017**, *164* (4), F387.
(97) Moussallem, I.; Jörissen, J.; Kunz, U.; Pinnow, S.; Turek, T. Chlor-Alkali Electrolysis with Oxygen Depolarized Cathodes: History, Present Status and Future Prospects. *J. Appl. Electrochem.* **2008**, *38* (9), 1177−1194.
(98) Pollard, R.; Newman, J. Transient Behaviour of Porous Electrodes with High Exchange Current Densities. *Electrochim. Acta* **1980**, *25* (3), 315−321.
(99) Shaw, R. A. Modeling and Design for Electrochemical Carbon Dioxide Capture Systems. Ph.D. Thesis. Massachusetts Institute of Technology, 2019.
(100) Pletcher, D.; Walsh, F. C. *Industrial Electrochemisty*; Springer, 1993.
(101) Yang, H. S.; Park, J. H.; Ra, H. W.; Jin, C. S.; Yang, J. H. Critical Rate of Electrolyte Circulation for Preventing Zinc Dendrite Formation in a Zinc−Bromine Redox Flow Battery. *J. Power Sources* **2016**, *325*, 446−452.
(102) Stowe, H. M.; Hwang, G. S. Fundamental Understanding of CO2 Capture and Regeneration in Aqueous Amines from First-Principles Studies: Recent Progress and Remaining Challenges. *Ind. Eng. Chem. Res.* **2017**, *56* (24), 6887−6899.
(103) Yang, X.; Rees, R. J.; Conway, W.; Puxty, G.; Yang, Q.; Winkler, D. A. Computational Modeling and Simulation of CO2 Capture by Aqueous Amines. *Chem. Rev.* **2017**, *117* (14), 9524−9593.
(104) Tian, Z.; Dai, S.; Jiang, D. en. What Can Molecular Simulation Do for Global Warming? *Wiley Interdiscip. Rev. Comput. Mol. Sci.* **2016**, *6* (2), 173−197.
(105) Da Silva, E. F.; Svendsen, H. F. Ab Initio Study of the Reaction of Carbamate Formation from CO2 and Alkanolamines. *Ind. Eng. Chem. Res.* **2004**, *43* (13), 3413−3418.
(106) Shim, J. G.; Kim, J. H.; Jhon, Y. H.; Kim, J.; Cho, K. H. DFT Calculations on the Role of Base in the Reaction between CO2 and Monoethanolamine. *Ind. Eng. Chem. Res.* **2009**, *48* (4), 2172−2178.
(107) da Silva, E. F.; Svendsen, H. F. Computational Chemistry Study of Reactions, Equilibrium and Kinetics of Chemical CO2 Absorption. *Int. J. Greenh. Gas Control* **2007**, *1* (2), 151−157.
(108) Arstad, B.; Blom, R.; Swang, O. CO2 Absorption in Aqueous Solutions of Alkanolamines: Mechanistic Insight from Quantum Chemical Calculations. *J. Phys. Chem. A* **2007**, *111* (7), 1222−1228.
(109) Sumon, K. Z.; Bains, C. H.; Markewich, D. J.; Henni, A.; East, A. L. L. Semicontinuum Solvation Modeling Improves Predictions of Carbamate Stability in the CO2 + Aqueous Amine Reaction. *J. Phys. Chem. B* **2015**, *119* (37), 12256−12264.
(110) Xie, H.-B.; Zhou, Y.; Zhang, Y.; Johnson, J. K. Reaction Mechanism of Monoethanolamine with CO2 in Aqueous Solution from Molecular Modeling. *J. Phys. Chem. A* **2010**, *114*, 11844−11852.
(111) Hwang, G. S.; Stowe, H. M.; Paek, E.; Manogaran, D. Reaction Mechanisms of Aqueous Monoethanolamine with Carbon

https://doi.org/10.1021/acs.chemrev.2c00681
Chem. Rev. 2023, 123, 8069−8098

Dioxide: A Combined Quantum Chemical and Molecular Dynamics Study. *Phys. Chem. Chem. Phys.* **2015**, *17* (2), 831−839.
(112) Guido, C. A.; Pietrucci, F.; Gallet, G. A.; Andreoni, W. The Fate of a Zwitterion in Water from Ab Initio Molecular Dynamics: Monoethanolamine (MEA)-CO2. *J. Chem. Theory Comput.* **2013**, *9*, 28−32.
(113) Han, B.; Zhou, C.; Wu, J.; Tempel, D. J.; Cheng, H. Understanding CO2 Capture Mechanisms in Aqueous Monoethanolamine via First Principles Simulations. *J. Phys. Chem. Lett.* **2011**, *2* (6), 522−526.
(114) Sumon, K. Z.; Henni, A.; East, A. L. L. Molecular Dynamics Simulations of Proposed Intermediates in the CO2 + Aqueous Amine Reaction. *J. Phys. Chem. Lett.* **2014**, *5* (7), 1151−1156.
(115) Ma, C.; Pietrucci, F.; Andreoni, W. Capture and Release of CO2 in Monoethanolamine Aqueous Solutions: New Insights from First-Principles Reaction Dynamics. *J. Chem. Theory Comput.* **2015**, *11* (7), 3189−3198.
(116) Matsuzaki, Y.; Yamada, H.; Chowdhury, F. A.; Higashii, T.; Onoda, M. Ab Initio Study of CO2 Capture Mechanisms in Aqueous Monoethanolamine: Reaction Pathways for the Direct Interconversion of Carbamate and Bicarbonate. *J. Phys. Chem. A* **2013**, *117* (38), 9274−9281.
(117) Orestes, E.; Machado Ronconi, C.; Carneiro, J. W. de M. Insights into the Interactions of CO2 with Amines: A DFT Benchmark Study. *Phys. Chem. Chem. Phys.* **2014**, *16* (32), 17213−17219.
(118) Mindrup, E. M.; Schneider, W. F. Computational Comparison of the Reactions of Substituted Amines with CO2. *ChemSusChem* **2010**, *3* (8), 931−938.
(119) Gangarapu, S.; Wierda, G. J.; Marcelis, A. T. M.; Zuilhof, H. Quantum Chemical Studies on Solvents for Post-Combustion Carbon Dioxide Capture: Calculation of PKa and Carbamate Stability of Disubstituted Piperazines. *ChemPhysChem* **2014**, *15* (9), 1880−1886.
(120) Gangarapu, S.; Marcelis, A. T. M.; Zuilhof, H. Improving the Capture of CO2 by Substituted Monoethanolamines: Electronic Effects of Fluorine and Methyl Substituents. *ChemPhysChem* **2012**, *13* (17), 3973−3980.
(121) Jhon, Y. H.; Shim, J. G.; Kim, J. H.; Lee, J. H.; Jang, K. R.; Kim, J. Nucleophilicity and Accessibility Calculations of Alkanolamines: Applications to Carbon Dioxide Absorption Reactions. *J. Phys. Chem. A* **2010**, *114* (49), 12907−12913.
(122) Li, H. C.; Chai, J. Da; Tsai, M. K. Assessment of Dispersion-Improved Exchange-Correlation Functionals for the Simulation of CO2 Binding by Alcoholamines. *Int. J. Quantum Chem.* **2014**, *114* (12), 805−812.
(123) Dubois, D. L.; Miedaner, A.; Bell, W.; Smart, J. C. Electrochemical Concentration of Carbon Dioxide. In *Electrochemical and Electrocatalytic Reactions of Carbon Dioxide*; Sullivan, B. R., Ed.; Elsevier: Amsterdam, 1993; pp 94−117.
(124) Koval, C.; Poshusta, J.; Scovazzo, P.; Noble, R.; DuBois, D. Electrochemical Separation and Concentration of < 1% Carbon Dioxide from Nitrogen. *J. Electrochem. Soc.* **2003**, *150* (5), D91−D98.
(125) Clarke, L. E.; Leonard, M. E.; Hatton, T. A.; Brushett, F. R. Thermodynamic Modeling of CO2 Separation Systems with Soluble, Redox-Active Capture Species. *Ind. Eng. Chem. Res.* **2022**, *61* (29), 10531−10546.
(126) Mizen, M. B.; Wrighton, M. S. Reductive Addition of CO2 to 9,10-Phenanthrenequinone. *J. Electrochem. Soc.* **1989**, *136* (4), 941.
(127) Nagaoka, T.; Nishii, N.; Fujii, K.; Ogura, K. Mechanisms of Reductive Addition of CO2 to Quinones in Acetonitrile. *J. Electroanal. Chem.* **1992**, *322* (1−2), 383−389.
(128) Qiao, X.; Li, D.; Cheng, L.; Jin, B. Mechanism of Electrochemical Capture of CO2 via Redox Cycle of Chlorinated 1,4-Naphthoquinone in BMIMBF4: An in-Situ FT-IR Spectroelectrochemical Approach. *J. Electroanal. Chem.* **2019**, *845*, 126−136.
(129) Schmidt, M. H.; Miskelly, G. M.; Lewis, N. S. Effects of Redox Potential, Steric Configuration, Solvent, and Alkali Metal Cations on the Binding of Carbon Dioxide to Cobalt(I) and Nickel(I) Macrocycles. *J. Am. Chem. Soc.* **1990**, *112* (9), 3420−3426.
(130) Appel, A. M.; Newell, R.; DuBois, D. L.; Rakowski DuBois, M. Concentration of Carbon Dioxide by Electrochemically Modulated Complexation with a Binuclear Copper Complex. *Inorg. Chem.* **2005**, *44* (9), 3046−3056.
(131) Ishida, H.; Ohba, T.; Yamaguchi, T.; Ohkubo, K. Interaction between CO < SUB > 2</SUB> and Electrochemically Reduced Species of N-Propyl-4,4′-Bipyridinium Cation. *Chem. Lett.* **1994**, *23*, 905−908.
(132) Singh, P.; Tarakeshwar, P.; Buttry, D. A. Experimental, Simulation, and Computational Study of the Interaction of Reduced Forms of N-Methyl-4,4'-Bipyridinium with CO2. *ChemElectroChem.* **2020**, *7* (2), 469−475.
(133) Ranjan, R.; Olson, J.; Singh, P.; Lorance, E. D.; Buttry, D. A.; Gould, I. R. Reversible Electrochemical Trapping of Carbon Dioxide Using 4,4′-Bipyridine That Does Not Require Thermal Activation. *J. Phys. Chem. Lett.* **2015**, *6* (24), 4943−4946.
(134) Singh, P.; Rheinhardt, J. H.; Olson, J. Z.; Tarakeshwar, P.; Mujica, V.; Buttry, D. A. Electrochemical Capture and Release of Carbon Dioxide Using a Disulfide-Thiocarbonate Redox Cycle. *J. Am. Chem. Soc.* **2017**, *139* (3), 1033−1036.
(135) Namazian, M.; Zare, H. R.; Yousofian-Varzaneh, H. Electrochemical Behavior of Tetrafluoro-p-Benzoquinone at the Presence of Carbon Dioxide: Experimental and Theoretical Studies. *Electrochim. Acta* **2016**, *196*, 692−698.
(136) Comeau Simpson, T.; Durand, R. R. Reactivity of Carbon Dioxide with Quinones. *Electrochim. Acta* **1990**, *35* (9), 1399−1403.
(137) Gupta, N.; Linschitz, H. Hydrogen-Bonding and Protonation Effects in Electrochemistry of Quinones in Aprotic Solvents. *J. Am. Chem. Soc.* **1997**, *119* (27), 6384−6391.
(138) De Sousa Bulhõesw, L. O.; Zara, A. J. The Effect of Carbon Dioxide on the Electroreduction of 1,4-Benzoquinone. *J. Electroanal. Chem. Interfacial Electrochem.* **1988**, *248* (1), 159−165.
(139) Zito, A. M.; Bím, D.; Vargas, S.; Alexandrova, A. N.; Yang, J. Y. Computational and Experimental Design of Quinones for Electrochemical CO2 Capture and Concentration. *ACS Sustain. Chem. Eng.* **2022**, *10* (34), 11387−11395.
(140) Schimanofsky, C.; Wielend, D.; Kröll, S.; Lerch, S.; Werner, D.; Gallmetzer, J. M.; Mayr, F.; Neugebauer, H.; Irimia-Vladu, M.; Portenkirchner, E.; et al. Direct Electrochemical CO2 Capture Using Substituted Anthraquinones in Homogeneous Solutions: A Joint Experimental and Theoretical Study. *J. Phys. Chem. C* **2022**, *126*, 14138−14154.
(141) Connelly, N. G.; Geiger, W. E. Chemical Redox Agents for Organometallic Chemistry. *Chem. Rev.* **1996**, *96* (2), 877−910.
(142) Barlow, J. M.; Yang, J. Y. Oxygen Stable Electrochemical CO2 Capture and Concentration with Quinones through Alcohol Additives. *J. Am. Chem. Soc.* **2022**, *144* (31), 14161−14169.
(143) Bui, A. T.; Hartley, N. A.; Thom, A. J. W.; Forse, A. C. Trade-Off between Redox Potential and the Strength of Electrochemical CO2 Capture in Quinones. *J. Phys. Chem. C* **2022**, *126* (33), 14163−14172.
(144) Alherz, A. W.; Petersen, H. A.; Singstock, N. R.; Sur, S. N.; Musgrave, C. B.; Luca, O. R. Predictive Energetic Tuning of Quinoid O-Nucleophiles for the Electrochemical Capture of Carbon Dioxide. *Energy Adv.* **2022**, *1* (11), 900−907.
(145) Petersen, H. A.; Alherz, A. W.; Stinson, T. A.; Huntzinger, C. G.; Musgrave, C. B.; Luca, O. R. Predictive Energetic Tuning of C-Nucleophiles for the Electrochemical Capture of Carbon Dioxide. *iScience* **2022**, *25* (4), No. 103997.
(146) Zanello, P. *Inorganic Electrochemistry*; Royal Society of Chemistry: Cambridge, 2003.
(147) Fan, H.; Cheng, L.; Jin, B. Investigation on Electrochemical Capture of CO2 in P-Benzoquinone Solutions by in Situ FT-IR Spectroelectrochemistry. *Electrochim. Acta* **2019**, *324*, No. 134882.
(148) Voskian, S.; Hatton, T. A. Faradaic Electro-Swing Reactive Adsorption for CO2 Capture. *Energy Environ. Sci.* **2019**, *12*, 3530−3547.
(149) Liu, Y.; Ye, H.-Z.; Diederichsen, K. M.; Van Voorhis, T.; Hatton, T. A. Electrochemically Mediated Carbon Dioxide Separation

https://doi.org/10.1021/acs.chemrev.2c00681
Chem. Rev. 2023, 123, 8069−8098

with Quinone Chemistry in Salt-Concentrated Aqueous Media. *Nat. Commun.* **2020**, *11*, 2278.
(150) Nagaoka, T.; Okazaki, S.; Fujinaga, T. Ion-Pair Effects on the Electroreduction of Carbonyl Compounds in N,-Dimethylformamide. *J. Electroanal. Chem.* **1982**, *133* (1), 89−99.
(151) Kim, Y. R.; Kim, R. S.; Kang, S. K.; Choi, M. G.; Kim, H. Y.; Cho, D.; Lee, J. Y.; Chang, S. K.; Chung, T. D. Modulation of Quinone PCET Reaction by Ca2+ Ion Captured by Calix[4]Quinone in Water. *J. Am. Chem. Soc.* **2013**, *135* (50), 18957−18967.
(152) Peover, M. E.; Davies, J. D. The Influence of Ion-Association on the Polarography of Quinones in Dimethylformamide. *J. Electroanal. Chem.* **1963**, *6*, 46−53.
(153) Delgado, M.; Wolf, R. E.; Hartman, J. R.; McCafferty, G.; Yagbasan, R.; Rawle, S. C.; Watkin, D. J.; Cooper, S. R. Redox-Active Crown Ethers. Electrochemical and Electron Paramagnetic Resonance Studies on Alkali Metal Complexes of Quinone Crown Ethers. *J. Am. Chem. Soc.* **1992**, *114*, 8983.
(154) Eggins, B. R. Interpretation of Electrochemical Reduction and Oxidation Waves of Quinone-Hydroquinone System in Acetonitrile. *J. Chem. Soc. D: Chem. Commun.* **1969**, *1969*, 1267−1268.
(155) Aimoto, Y.; Koshiba, K.; Yamauchi, K.; Sakai, K. A Family of Molecular Nickel Hydrogen Evolution Catalysts Providing Tunable Overpotentials Using Ligand-Centered Proton-Coupled Electron Transfer Paths. *Chem. Commun.* **2018**, *54* (91), 12820−12823.
(156) Diederichsen, K. M.; Liu, Y.; Ozbek, N.; Seo, H.; Hatton, T. A. Toward Solvent-Free Continuous-Flow Electrochemically Mediated Carbon Capture with High-Concentration Liquid Quinone Chemistry. *Joule* **2022**, *6* (1), 221−239.
(157) Kajiwara, T.; Yamaguchi, T.; Kido, H.; Kawabata, S.; Kuroda, R.; Ito, T. A Dinucleating Bis(Dimethylcyclam) Ligand and Its Dinickel(II) and Dizinc(II) Complexes with the Face-to-Face Ring Arrangement. *Inorg. Chem.* **1993**, *32* (23), 4990−4991.
(158) Murase, I.; Vučkovic, G.; Kodera, M.; Harada, H.; Matsumoto, N.; Kida, S. Synthesis and Characterization of Copper(II), Nickel(II), and Cobalt(II) Binuclear Complexes with a New Tricyclic Octadentate Ligand, 1,5,8,12,15,19,22,26-Octaazatricyclo-[17.9.2.25,5]Dotriacontane (Tcoa): Trapping of CO2 in a Neutral Aqueous Solution. *Inorg. Chem.* **1991**, *30* (4), 728−733.
(159) Harada, H.; Kodera, M.; Vučković, G.; Matsumoto, N.; Kida, S. Preparation and Redox Chemistry of Novel Carbonato-Bridged Cobalt(II) Complexes with 1,4,8,11 -Tetrakis (2-Aminoethyl)-1,4,8,11 -Tetraazacyclotetradecane and 1,4,8,11-Tetrakis-(Pyridylmethyl)-1,4,8,11-Tetraazacyclotetradecane. *Inorg. Chem.* **1991**, *30* (6), 1190−1194.
(160) Newell, R.; Appel, A.; DuBois, D. L.; Rakowski DuBois, M. Studies of Bicarbonate Binding by Dinuclear and Mononuclear Ni(II) Complexes. *Inorg. Chem.* **2005**, *44*, 365−373.
(161) Li, X.; Zhao, X.; Liu, Y.; Hatton, T. A.; Liu, Y. Redox-Tunable Lewis Bases for Electrochemical Carbon Dioxide Capture. *Nat. Energy* **2022**, *7* (11), 1065−1075.
(162) Stueber, D.; Orendt, A. M.; Facelli, J. C.; Parry, R. W.; Grant, D. M. Carbonates, Thiocarbonates, and the Corresponding Monoalkyl Derivatives: III. The 13C Chemical Shift Tensors in Potassium Carbonate, Bicarbonate and Related Monomethyl Derivatives. *Solid State Nucl. Magn. Reson.* **2002**, *22* (1), 29−49.
(163) Stueber, D.; Arif, A. M.; Grant, D. M.; Parry, R. W. Carbonates, Thiocarbonates, and the Corresponding Monoalkyl Derivatives. 2. X-Ray Crystal Structure of Potassium Methyltrithiocarbonate (KS2CSCH3). *Inorg. Chem.* **2001**, *40* (8), 1912−1914.
(164) Harris, D.; Bushnell, E. Density Functional Theory Study of the Capture and Release of Carbon Dioxide by Benzyl-Disulfide, -Diselenide, and -Ditelluride. *J. Phys. Chem. A* **2019**, *123* (15), 3383−3388.
(165) Gangi, D. A.; Durand, R. R. Binding of Carbon Dioxide to Cobalt and Nickel Tetra-Aza Macrocycles. *J. Chem. Soc., Chem. Commun.* **1986**, 697−699.
(166) Bard, A. J.; Faulkner, L. R. *Electrochemical Methods: Fundamentals and Applications*, 2nd ed.; Wiley, 2001.
(167) Creutz, C. Carbon Dioxide Binding To Transition-Metal Centers. In *Electrochemical and Electrocatalytic Reactions of Carbon Dioxide*; Sullivan, B. R., Ed.; Elsevier: Amsterdam, 1993; pp 19−67.
(168) Creutz, C.; Schwarz, H. A.; Wishart, J. F.; Fujita, E.; Sutin, N. Thermodynamics and Kinetics of Carbon Dioxide Binding to Two Stereoisomers of a Cobalt(I) Macrocycle in Aqueous Solution. *J. Am. Chem. Soc.* **1991**, *113* (9), 3361−3371.
(169) Benesi, H. A.; Hildebrand, J. H. A Spectrophotometric Investigation of the Interaction of Iodine with Aromatic Hydrocarbons. *J. Am. Chem. Soc.* **1949**, *71* (8), 2703−2707.
(170) Bains, P.; Psarras, P.; Wilcox, J. CO2 Capture from the Industry Sector. *Prog. Energy Combust. Sci.* **2017**, *63*, 146−172.

https://doi.org/10.1021/acs.chemrev.2c00681
Chem. Rev. 2023, 123, 8069−8098